SCIENCE CHINA
Earth Sciences

•ARTICLE•

March 2024 Vol.67 No.3: 826–842
https://doi.org/10.1007/s11430-023-1273-1

Coupled conditional nonlinear optimal perturbations and their application to ENSO ensemble forecasts

Wansuo DUAN[1,2*], Lei HU[1,2] & Rong FENG[1]

[1] *LASG, Institute of Atmospheric Physics, Chinese Academy of Sciences, Beijing 100029, China;*
[2] *University of Chinese Academy of Sciences, Beijing 100049, China*

Received August 4, 2023; revised January 27, 2024; accepted February 7, 2024; published online February 26, 2024

Abstract Limitations are existed in current ensemble forecasting initial perturbation methods for describing the interactions among various spheres of the Earth system. In this study, a new method is proposed, namely, the coupled conditional nonlinear optimal perturbation (C-CNOP) method, which incorporates multisphere interactions much appropriately. The El Niño-Southern Oscillation (ENSO) is a typical ocean-atmosphere "coupling" (or "interaction") phenomenon. The C-CNOP method is applied to ensemble forecasting of ENSO. It is demonstrated that the C-CNOP method can generate coupled initial perturbations (CPs) that appropriately consider initial ocean-atmosphere coupling uncertainty for ENSO ensemble forecasts. Results reveal that the CPs effectively improve the ability of ENSO ensemble-mean forecasts in both temporal variability of Niño3.4 sea surface temperature anomalies (SSTAs) and spatial variability of ENSO mature-phase SSTAs. Notably, despite the weakest ocean-atmosphere coupling strength in the tropical Pacific occurring during the boreal spring and summer, CPs still capture the uncertainties of this weak coupling when ENSO predictions are initialized at these seasons. This performance of CPs significantly suppresses the rapid increase of ENSO prediction errors due to the high ocean-atmosphere coupling instability during these seasons, and thus effectively extends the lead time of skillful ENSO forecasting. Hence, the C-CNOP method is a suitable initial perturbation approach for ENSO ensemble forecast that can describe initial ocean-atmosphere coupling uncertainty. It is expected that the C-CNOP method plays a significant role in predictions of other high-impact climate phenomena, and even future Earth system predictions.

Keywords Ensemble forecast, Multisphere interaction, Initial perturbations, ENSO

Citation: Duan W, Hu L, Feng R. 2024. Coupled conditional nonlinear optimal perturbations and their application to ENSO ensemble forecasts. Science China Earth Sciences, 67(3): 826–842, https://doi.org/10.1007/s11430-023-1273-1

1. Introduction

Ensemble forecasting is a vital approach for estimating the uncertainty in weather and climate predictions and improving the accuracy of numerical forecasts. The World Meteorological Organization (WMO) has recognized this approach as a key development strategy for future numerical weather forecasting. The quality of ensemble forecasts depends on how the initial perturbation samples are generated (Du et al., 2018). Previous studies have indicated that only by superimposing growing-type initial perturbations on control forecasts can achieve much higher ensemble forecasting skill (Toth and Kalnay, 1993; Duan et al., 2023a, 2023b). Regarding climate predictions that require considering multisphere interaction of the Earth system, such growing-type initial perturbations must also reflect the effect of multisphere coupling uncertainties to further improve the level of climate predictions. Currently, the widely popular methods for generating growing-type initial perturbations are the bred vector (BV) method (Toth and Kalnay, 1993) and the singular vector (SV) method (Mureau et al., 1993; Buizza and Palmer, 1995; Molteni et al., 1996). The BV method had

* Corresponding author (email: duanws@lasg.iap.ac.cn)

been applied in the ensemble forecasting system of the National Centers for Environmental Prediction (NCEP) in the U.S. in 1992. The SV method has been adopted by the European Centre for Medium-Range Weather Forecasts (ECMWF) for ensemble forecasting, which leads to tremendous success in numerical weather forecasting. Moreover, the SV method is so far still one of the fundamental ensemble forecasting methods of the ECMWF (https://confluence.ecmwf.int/display/FUG/). Even though BV and SV methods exhibit their own advantages, the initial perturbations generated are insufficient for fully characterizing multisphere coupling uncertainties (Kleeman et al., 2003; Vannitsem and Duan, 2020). The BVs of a coupled system are generated by breeding from an initial guess of perturbations, whose components possess different variabilities, but they often identify a kind of growing-type initial perturbations only responsible for the time period before the forecast period (Du et al., 2019; Duan et al., 2023a). This shortcoming results in that the BVs obtain a skillful ensemble forecasting only for a very short lead time (Zhang et al., 2023). Furthermore, Vannitsem and Duan (2020) applied the backward Lyapunov vector (BLV) method, which is similar to the BV method but independent of breeding parameters, to obtain ensemble forecasts with a reduced-order multiscale coupled ocean-atmosphere model. They revealed that the fastest-growing BLVs primarily reflect fast atmospheric variability, while the slowly growing or nongrowing BLV modes predominantly reflect slow oceanic variability. If the fast-growing BLVs, generally needed to achieve a high ensemble forecasting skill for atmosphere, are adopted to initialize the coupled system, it is not conducive to improving the ensemble forecasting ability of coupled ocean-atmosphere events. The SV method of the ECMWF model characterizes the fast-growing perturbations on control forecasts within the forecast period, and exhibits reasonable dynamics, which may be one of the reasons why the SV method has achieved tremendous success in numerical weather forecasting (Du et al., 2019; Duan et al., 2023a, 2023b). However, it is undeniable that SVs are obtained based on linear error growth assumption, which cannot fully reflect the effect of nonlinear processes (Mu et al., 2003); furthermore, SVs cannot describe the coupling uncertainties of different sphere variabilities (Kleeman et al., 2003).

Considering the linear limitation of SVs, Duan and Huo (2016) proposed a new ensemble forecasting method, namely, the orthogonal conditional nonlinear optimal perturbation (O-CNOP) method. The O-CNOP method not only considers the influence of nonlinear physical processes, but also characterizes the fast-growing initial perturbations on the control forecast within the forecast period. Therefore, the O-CNOP has reasonable dynamics. This method has been applied in ensemble forecasting of typhoon tracks. It not only effectively reduces the forecast errors of typhoon tracks, but also yields higher forecasting accuracy than traditional SV and BV methods in determining the typhoon landfall location, landfall time, and even track turning (Huo and Duan, 2018; Huo et al., 2019; Duan et al., 2023a, 2023b; Zhang et al., 2023). However, similar to the SV method, it is highly challenging to apply the O-CNOP method in the consideration of the effect of multisphere coupling uncertainties when applied to a coupled model. Given the limitation of the O-CNOP method while considering its advantage in characterizing nonlinear-growth initial perturbations during the forecast period, the aim of this study is to develop a new initial perturbation method for ensemble forecasting that generalizes O-CNOPs to consider coupling uncertainties. This method is hereafter referred to as the coupled conditional nonlinear optimal perturbation (C-CNOP) method.

The ENSO, as a tropical ocean-atmosphere coupled phenomenon with the strongest interannual variability signal, often leads to abnormal weather and climate conditions in China and even globally, causing severe natural disasters. It has attracted widespread attention from governments and the public. Therefore, accurate prediction of ENSO events is highly important (Lian et al., 2023). However, publically recognized skillful ENSO forecasting has only a 6-month lead time (Tang et al., 2018; Duan et al., 2022, 2023a). Therefore, significant improvements in the ENSO forecasting skill and the extension of the forecast lead time are urgently important, which could be beneficial for governments to effectively formulate disaster prevention and reduction measures in advance and rationally deploy national social and economic activities.

In many studies, ensemble forecasts of ENSO have been conducted by perturbing the atmosphere or ocean alone or by simultaneously but separately generating initial oceanic and atmospheric perturbations (Yan et al., 2009; Duan and Wei, 2013; Du et al., 2012; Baehr and Piontek, 2014). However, such initial perturbations cannot fully reflect the effect of coupling ocean-atmosphere uncertainties. Then, if these effects are properly considered in ENSO ensemble forecasting, whether or not the forecasting ability can be significantly improved? In particular, previous research has indicated that the strength of ocean-atmosphere coupling in the tropical Pacific is lowest during the boreal spring and summer seasons; nevertheless, current numerical models can hardly capture this weak coupling; consequently, when predicting the ENSO starting in spring and summer, the initial fields fail to adequately incorporate this weak coupling information (Webster, 1995; Zheng and Zhu, 2010). Hence, if fast-growing initial perturbations of ENSO ensemble forecasts can better capture the uncertainties of the lowest coupling signal in spring and summer, will the ENSO forecast skill be effectively improved? To address the aforementioned question, the C-CNOP method is used for ENSO ensemble forecasting to explore the effect of the initial coupling un-

certainty on the ENSO ensemble forecasting skill.

2. Coupled conditional nonlinear optimal perturbations

Climate variability is caused by multisphere interactions involving the atmosphere, ocean, land, and other spheres, and each sphere exhibits its characteristic variability. Therefore, in numerical forecasting of climate variability, Earth-climate system coupled models should be adopted. However, because of the limitations at the current cognitive level, existing coupled models cannot accurately depict the mechanisms of multisphere interactions, resulting in high uncertainties in climate forecasting. Thus, the growing-type initial perturbations employed for ensemble forecasting, as stated in the introduction, must also account for multisphere coupling uncertainties for achieving higher forecast skills when using coupled models. Therefore, how can fast-growing initial perturbations for ensemble forecasts be generated that properly incorporate multisphere coupling uncertainties?

To answer the above question, we abstract the multisphere coupled dynamical system as a conceptual model that includes the interaction between fast-varying variables (such as synoptic-scale variability in the atmosphere) and slow-varying variables (such as climate variability in the ocean); specifically, we consider the following nonlinear partial differential equations:

$$\begin{cases} \dfrac{\partial X}{\partial t} = F(X,Y,t) + f_X, \\ \dfrac{\partial Y}{\partial t} = \dfrac{1}{\epsilon} G(X,Y,t) + f_Y, \\ U_0 = \left(X|_{t=0} = X_0,\ \ Y|_{t=0} = Y_0\right), \Omega \times [0,T], \end{cases} \tag{1}$$

where, X and Y are the slow- and fast-varying variables, respectively, $U_0 = (X_0, Y_0)$ denotes their initial state, t is the time, with $t \in [0,T]$, $T < +\infty$, F and G are nonlinear functionals, f_X and f_Y denote the external forcings of the slow-varying variables (such as tides, sea surface heat fluxes and freshwater fluxes in ocean) and fast-varying variables (such as solar radiation, carbon dioxide concentration and aerosols in atmosphere), and $\epsilon \ll 1$ is applied to distinguish the slow-varying variable X and the fast-varying variable Y in eq. (1).

When forecasting the slow-varying variable X (such as the ocean temperature in the climate system), the differential equation for the slow-varying variable in eq. (1) can be expressed as follows:

$$\mathrm{d}X = F(X,Y,t)\mathrm{d}t + f_X\,\mathrm{d}t. \tag{2}$$

Assuming that both f_X and f_Y are constant external forcings (e.g., preindustrial external forcings in the international coupled model intercomparison project (CMIP) experiments), we therefore have the indication of considering only the effect of the internal variability of fast- and slow-varying variables. The integration of eq. (2) over the time interval $[t_a,t_b](t_a < t_b \leqslant T)$ can be derived as in eq. (3):

$$\begin{aligned} \int_{t_a}^{t_b} \mathrm{d}X &= \int_{t_a}^{t_b} F(X,Y,t)\mathrm{d}t + \int_{t_a}^{t_b} f_X\,\mathrm{d}t \\ &= \int_{t_a}^{t_b} F(X,Y,t)\mathrm{d}t + f_X(t_b - t_a). \end{aligned} \tag{3}$$

Therefore, the slow-varying variable X_{t_b} at future time t_b can be described as follows:

$$X_{t_b} = X_{t_a} + \int_{t_a}^{t_b} F(X,Y,t)\mathrm{d}t + f_X(t_b - t_a). \tag{4}$$

Note that Y_{t_b} also needs to be calculated when solving the eq. (4). In fact, Y_{t_b} can be derived by eq. (5) similar to eq. (4):

$$Y_{t_b} = Y_{t_a} + \frac{1}{\epsilon}\int_{t_a}^{t_b} G(X,Y,t)\mathrm{d}t + f_Y(t_b - t_a). \tag{5}$$

For convenience, the initial state in eqs. (4) and (5) is denoted as $U_{t_a} = \left(X_{t_a}, Y_{t_a}\right)$, and the final state is represented by $U_{t_b} = \left(X_{t_b}, Y_{t_b}\right)$.

According to eqs. (4) and (5), if we select two periods $[t_{01}, t_1]$ and $[t_{02}, t_2]$ from time series of coupled model output with initial states denoted as $U_{t_{01}} = \left(X_{t_{01}}, Y_{t_{01}}\right)$ and $U_{t_{02}} = \left(X_{t_{02}}, Y_{t_{02}}\right)$, respectively, the final states of the slow-varying variables X_{t_1} and X_{t_2} can be written as follows:

$$X_{t_1} = \int_{t_{01}}^{t_1} F\mathrm{d}t + X_{t_{01}} + f_X(t_1 - t_{01}), \tag{6}$$

$$X_{t_2} = \int_{t_{02}}^{t_2} F\mathrm{d}t + X_{t_{02}} + f_X(t_2 - t_{02}). \tag{7}$$

If the two periods are of the same length, eq. (7) minus eq. (6) can be expressed as in eq. (8).

$$X_{t_2} - X_{t_1} = X_{t_{02}} - X_{t_{01}} + \left(\int_{t_{02}}^{t_2} F\mathrm{d}t - \int_{t_{01}}^{t_1} F\mathrm{d}t\right). \tag{8}$$

Eq. (8) can be rewritten in the eq. (9), which has the same form as eqs. (6) and (7).

$$X_{t_2} - X_{t_1} = X_{t_{02}} - X_{t_{01}} + \int_{\Sigma}\left[F_{t_{02}} - F_{t_{01}}\right]\mathrm{d}t. \tag{9}$$

where, $F_{t_{02}}$ is the F in eq. (7), with the corresponding integral interval Σ matching the time interval of $[t_{01}, t_1]$, and $F_{t_{01}}$ is the F in eq. (6), with the integration interval Σ equaling $[t_{01}, t_1]$; in particular, Y_{t_2} and Y_{t_1} in eq. (9) can be calculated by eq. (5).

Eqs. (8) and (9) reveal that the difference between X_{t_1} and X_{t_2} stems from the difference between $U_{t_{01}}$ and $U_{t_{02}}$. In other

words, the differences in the initial states of the slow-varying variable X and fast-varying variable Y jointly leads to the differences of the slow-varying variable in the future. Therefore, if the data series within the period $[t_{01}, t_1]$ is regarded as an observation series, the data series within the period $[t_{02}, t_2]$ can be regarded as the prediction series of the observation series. Then the prediction error at the termination time is due to the difference between $U_{t_{02}}$ and $U_{t_{01}}$, namely, the initial errors $(X_{t_{02}} - X_{t_{01}}, Y_{t_{02}} - Y_{t_{01}})$ of the slow- and fast-varying variables, respectively.

For a given time series, considering the initial error that leads to the maximum forecast error, the following optimization problem can be established:

$$J(u_{i,n}) = \mathrm{MAX}(1 \leqslant n < N; i < N) \parallel X_{T_{i,n}} - X_{T_i} \parallel, \quad (10)$$

where, $u_{i,n} = (x_{i,n}, y_{i,n})$ represents the initial error that can lead to the maximum forecast error at forecast time T based on the i-th observation series and its n prediction series. $n < N$ indicates the number of prediction series and can be widely selected from the model data series to ensure the diversity of the prediction series. Therefore, the initial error $u_{i,n}$ obtained from eq. (10) is based on a finite number of prediction sequences but causes a statistically significant result, especially includes the effects of the interactions between the fast- and slow-varying variables.

As stated in the Introduction, CNOP represents the initial perturbation that satisfies certain physical constraints and causes the largest prediction error at the forecast time (Mu et al., 2003). Regarding eq. (10), if the above limited number of but statistically significant samples of the prediction sequences are adopted as constraints, eq. (10) provides the statistically optimal coupled CNOP, denoted as C-CNOP.

The above C-CNOP is derived based on the predictions of slow-varying variables. In fact, we can similarly deduce the C-CNOP for predicting fast-varying variables. Furthermore, one can extend this concept to more general situations of multisphere interactions in the Earth system for research needs. Therefore, C-CNOP could provide a method to produce optimal initial perturbations that not only much appropriately take into account multi-sphere interactions, but also much effectively enhance the forecasting level for weather-climate seamless predictions. For the sake of simplicity, additional details are not provided here.

3. Application of the C-CNOP method in ENSO ensemble forecasting

In this section, the C-CNOP method is applied to the Community Earth System Model (CESM), and its ability to facilitate ENSO forecasting is investigated by considering the impact of ocean-atmosphere coupling uncertainties on the optimal initial perturbations of the ensemble forecasts.

3.1 Model and Data

The CESM was developed by the National Center for Atmospheric Research (NCAR). It is a fully coupled Earth system model that comprises atmospheric, oceanic, land, sea ice, and land ice components. Regarding the atmospheric component, the Community Atmosphere Model 5 (CAM5; Neale et al., 2010) contains a finite-volume (FV) dynamic core with 30 vertical layers and a horizonal resolution of 0.9°×1.25° (longitude × latitude). The oceanic component is based on the Parallel Ocean Program (POP) version (Smith et al., 2010), which provides 60 vertical levels with a layer spacing ranging from 10 m in the upper 150 m to 250 m below 4000 m, and a horizontal resolution of 1°×0.27° (longitude × latitude) at the equator, with the domain ranging from 79°S to 89°N. It uses a displaced pole grid in the Northern Hemisphere and spherical coordinates in the Southern Hemisphere. In addition, the sea ice component model, i.e., Community Ice Code version 4 (Hunke and Lipscomb, 2008), and the land surface model, i.e., Community Land Model version 4 (Oleson et al., 2010), are adopted in the CESM. The component models of the CESM are coupled through the version 7 coupler (CPL7; Craig et al., 2012).

In this study, the Global Ocean Data Assimilation System (GODAS) dataset is utilized, which is retrieved from the National Centers for Environmental Prediction (NCEP) of the National Oceanic and Atmospheric Administration (NOAA). This dataset is currently the most widely used real-time ocean assimilation dataset. With the use of the nudging method, we assimilate sea temperature data from the GODAS into the initial field of the CESM ocean model and obtain initial analysis fields of the predictions made by the CESM. The assimilation area covers the global ocean horizontally, and the vertical direction extends from 15 to 400 m in the deep layer. The assimilation period ranges from 1980 to 2015. With the use of the initial analysis, forecasts of the sea temperature in the tropical Pacific are obtained by integrating the CESM. For convenience, these forecasts are hereafter referred to as control forecasts (denoted by "Ctrl" in the figures).

3.2 Coupled initial perturbations generated by the C-CNOP method for ENSO ensemble forecasting

Duan et al. (2018) demonstrated that the spatial pattern of the fastest-growing initial errors of ENSO events (whether El Niño or La Niña) is independent of the events themselves, but is sensitive to the forecast start time (Mu et al., 2007a, 2007b; Duan et al., 2009; Hou et al., 2019). Therefore, if we extract the basis of the phase space for the fast-growing initial perturbations in the ensemble forecasts for ENSO from the above rapidly growing initial error modes generated for

different forecast start times, these bases characterize the major modes of the initial perturbations that significantly affect the ENSO. Based on the amplitude characteristics of the initial analysis errors of the control forecasts, one can utilize the linear combination of these base vectors to construct the phase space of the nonlinearly coupled rapid-growth initial perturbations in the ensemble forecasts at each start time. By using perturbation samples from this space, ENSO ensemble forecasting experiments can be conducted. In this section, we generate C-CNOPs for different ENSO events to construct a basis of the phase space for growing-type coupled initial perturbations in ensemble forecasting. Subsequently, we generate samples of initial perturbations for ENSO ensemble forecasting, and investigate the effect of these coupled initial perturbations on the ENSO ensemble forecasting skill.

The CESM is integrated for 200 years, with constant pre-industrial external forcing, and the last 150 years are applied to generate C-CNOPs. From these data, we choose 10 typical El Niño years that are warm during the early boreal spring and exhibit a peak temperature at the end of the year as observations. For each of these one-year observations, the remaining 149 years of the data sequence are assumed as the 149 predictions of the observations (with a lead time of 12 months), where the forecast errors are solely caused by the initial errors. The objective function $J(t)$ can be expressed as follows.

$$J(t)=\sqrt{\frac{1}{N}\sum_{(i,j)}\left[T^{p}_{(i,j)}(t)-T^{o}_{(i,j)}(t)\right]^{2}}, \tag{11}$$

$J(t)$ measures the forecast errors of the sea surface temperature (SST) in the tropical Pacific; T^{o} denotes the observed sea temperature, T^{p} signifies its prediction, (i,j) represents the grid points in the domain of the tropical Pacific (20°S–20°N, 120°E–80°W), and N is the total grid number in the tropical Pacific. Based on eq. (9), the C-CNOP for each prediction can be calculated, which covers the global ocean, including all components such as the ocean, atmosphere and land surface. This C-CNOP represents the coupled initial perturbation that imposes the greatest effect on the forecasting uncertainty of the tropical Pacific sea temperature in the CESM from a statistical perspective (see Section 2).

The ENSO ensemble forecasting experiments start in January, April, July and October of each year, with a lead time of 12 months. In each starting month, the corresponding prediction generates 1 C-CNOP, while the predictions of 10 El Niño observations generate 10 C-CNOPs. Based on these C-CNOPs, we continue to consider the second to fifth fast-growing initial perturbations of each prediction. Thus, a total of 50 fast-growing initial perturbations are obtained for the 10 observed El Niño at each start month, collectively denoted as C-CNOPs.

In this study, the effect of ocean-atmosphere coupled initial perturbations on the ENSO ensemble forecasting skill is investigated. Based on the 50 C-CNOPs obtained at a given start month, combined empirical orthogonal function decomposition (CEOF) is performed on the sea temperature component T_0 and the wind component U_0 and V_0 to obtain the 20 leading modes, denoted as $E_i=(T_{0i}, U_{0i}, V_{0i})$ (i=1, 2, 3, ... , 20; which explain more than 90% of the total variance). By linearly combining these 20 leading modes, we obtain the coupled perturbations of sea temperature and wind components, signified as CP=(IT_0, IU_0, IV_0)=a_1E_1+a_2E_2+…+$a_{20}E_{20}$, where a_i denotes constant coefficients. Obviously, CP is a fast-growing coupled initial perturbation of sea temperature and wind components. By selecting different coefficients a_i, different coupled initial perturbations can be obtained and used as perturbation samples for ENSO ensemble forecasting. As mentioned above, the CP amplitudes can be determined by using the amplitudes of the initial analysis errors at different starting months, which are measured using the L2 norm.

In this study, ENSO ensemble forecasting experiments from January 1982 to December 2015 are conducted. As the C-CNOP method proposed in this study is the first attempt at ENSO ensemble forecasting, we only experimentally generate 5 CPs for each prediction to validate the rationality of the C-CNOP method. The 5 CPs are added and subtracted from the initial analysis field of the control forecast (as described in Section 3); then, 10 perturbed forecasts are obtained by integrating the CESM, together with the control forecast, finally yielding a total of 11 ensemble members. The CPs cover the entire globe horizontally and comprise 17 layers of the sea temperature beneath the ocean surface, with a depth of up to 165 m, which is approximately the depth of the thermocline bottom in the equatorial Pacific. Simultaneously, the CPs include 19 layers of global wind fields vertically above the bottom boundary layer, with a height of up to nearly 200 hPa, which is approximately the height of the top of the Walker circulation in the equatorial Pacific. As an example of CPs, Figure 1 plots 5 CPs of the control forecast for the 1982/83 El Niño event starting from 1 April in the El Niño year. It is shown that the 5 CPs exhibit various patterns of the sea surface temperature (SST) and wind field; however, when the tropical Pacific exhibits a local cold SST anomaly (SSTA), the anomalous wind field primarily exhibits divergence; conversely, when there is a local warm SSTA, the anomalous wind field converges. According to the wind-evaporation-SST (WES; Xie and Philander, 1994) feedback mechanism, it is known that the interactions between sea temperature and wind field of the CPs are dynamically coordinated and incorporate the effect of ocean-atmosphere interaction in the tropical Pacific.

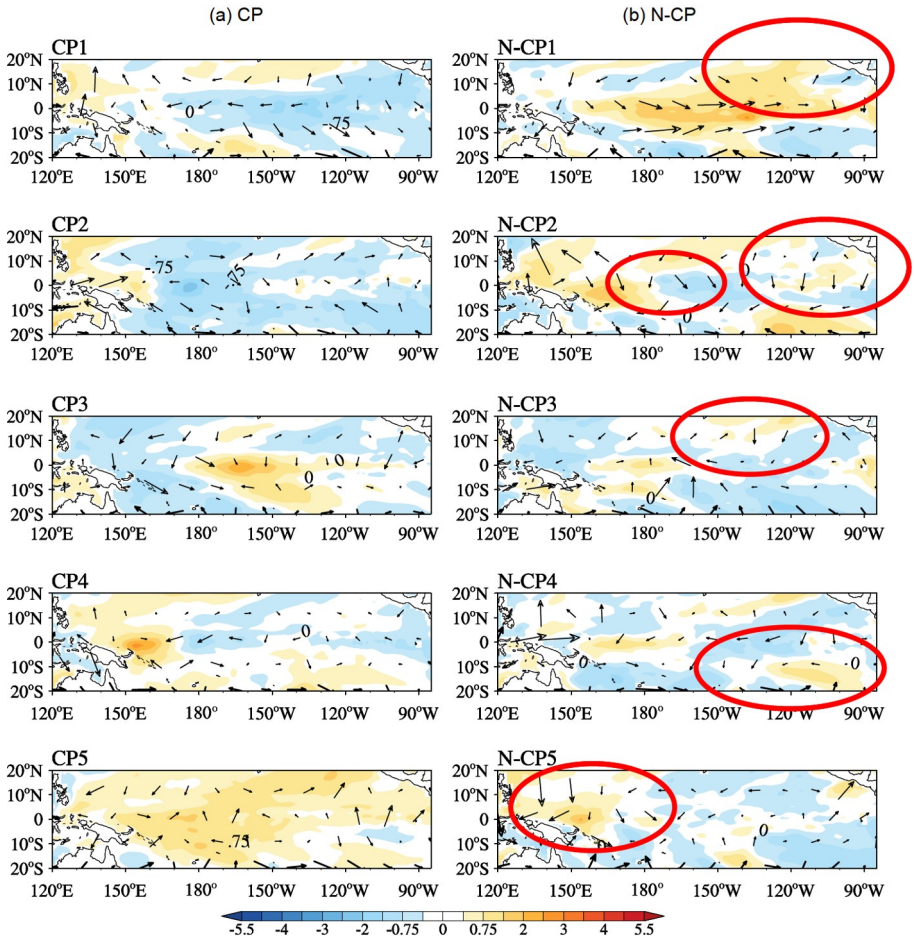

Figure 1 Spatial patterns of the five CPs (a) and N-CPs (b) of the control forecast for the 1982/1983 El Niño event at the start time of 1 April. The shaded areas denote SSTAs, and the arrows indicate wind vectors.

3.3 Ensemble forecasting of tropical Pacific SSTAs

We use the CPs to conduct ensemble forecasting for SSTAs with a 12-month lead time, where the CPs are generated at the start months of 1st January, 1st April, 1st July and 1st October from 1982 to 2015. A total of 136 predictions are produced We now investigate the effect of the initial coupling uncertainties described by CPs on the ENSO ensemble forecasting skill.

3.3.1 Forecast errors

Figure 2 shows the time series of the Niño3.4 SSTA (i.e., the Niño3.4 index) in the GODAS datasets and the ensemble-mean forecasts of the Niño3.4 index during the ENSO mature phase at 3-, 6-, 9- and 12-month lead times. The results demonstrate that both the control forecasts and the CP-ensemble mean forecasts can predict major El Niño and La Niña events well with a 9-month lead time, whereas the CP-ensemble mean forecasts are more accurate and achieve higher forecasting ability. Quantitatively, the CP-ensemble mean forecast errors (i.e., the root-mean-square errors [RMSEs]) are statistically reduced by more than 16% relative to the control forecasts for the Niño3.4 SSTA during all the ENSO mature phases from 1982 to 2015 at various lead times; in particular, at a lead time of 9 months, the CP-ensemble mean forecast errors are reduced by up to 25% relative to the control forecasts, and even reach 30% at a 6-month lead time (Figure 3).

To investigate the importance of simultaneously considering the initial uncertainties in both sea temperature and wind in improving ENSO ensemble forecasting skill, ensemble forecasting experiments are also performed with sea temperature and wind perturbed separately. To better describe the initial uncertainties represented by individual sea temperature or wind perturbations, we conduct empirical orthogonal function decomposition (EOF) of sea temperature and wind components of C-CNOPs, respectively, and select the leading 20 EOF modes for the sea temperature and the leading 20 combined EOF modes for zonal and meridional winds as the bases to produce the rapidly growing initial perturbations in ensemble forecasting. With the use of combinations of these bases, we generate initial sea temperature and wind perturbations for ensemble forecasting, denoted as CP-T and CP-W, respectively. Figure 1 shows five

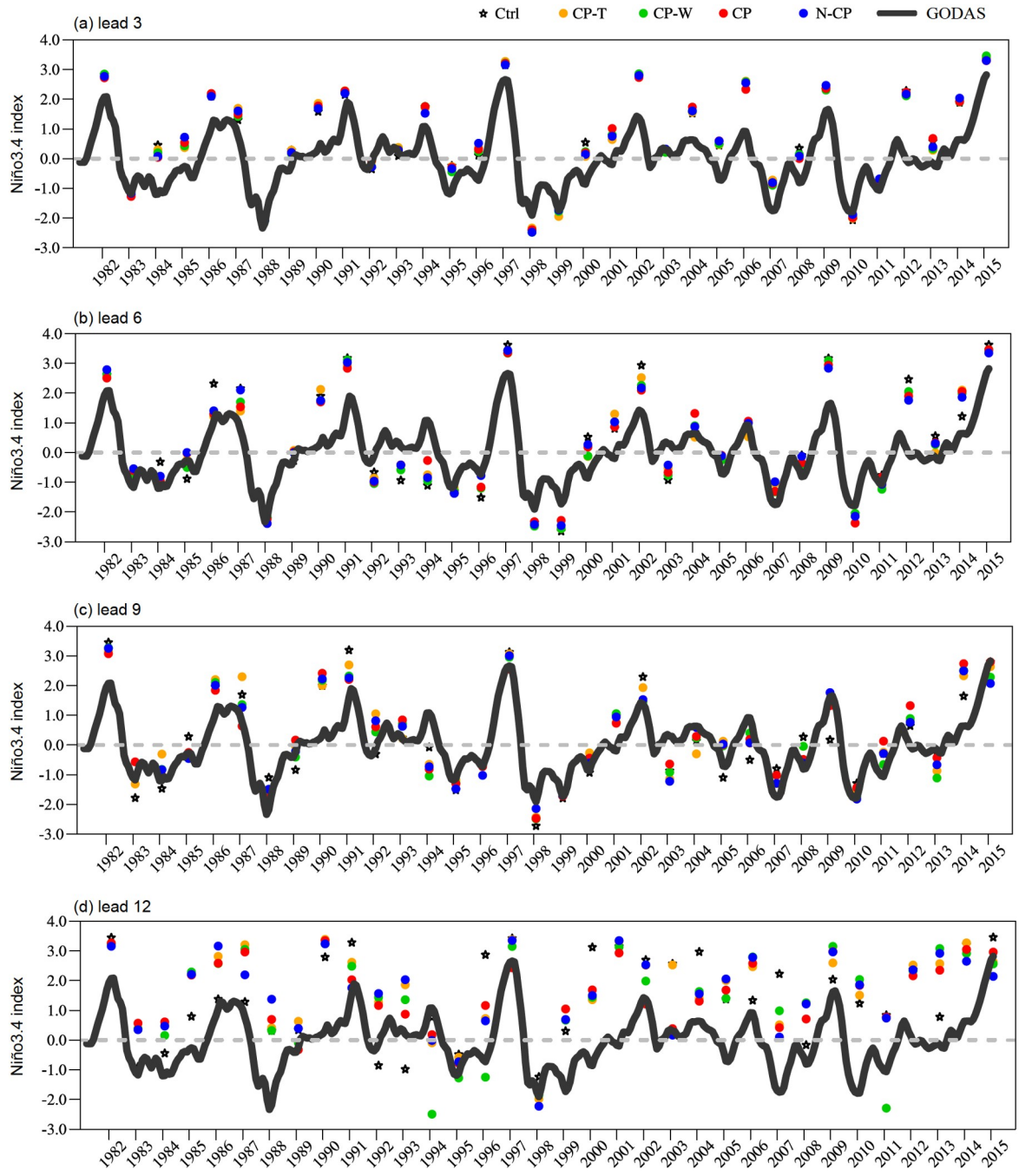

Figure 2 Time series of the observed Niño3.4 SSTAs and the ensemble mean forecasts for the mature phase Niño3.4 SSTAs from 1982 to 2015 at lead times of (a) 3, (b) 6, (c) 9 and (d) 12 months. The black curves indicate the observations; the red, blue, green and yellow dots represent the CP, N-CP, CP-W and CP-T ensemble mean forecasts, respectively; and the asterisks indicate the control forecasts.

CP-Ts and five CP-Ws (i.e., the SST and wind anomaly components of the N-CP) for the control forecasts of the 1982/1983 El Niño event starting on the 1 April in the El Niño year. The results show that, compared with sea temperature and wind components of CPs, CP-Ts and CP-Ws exhibit different perturbation patterns. Furthermore, CP-Ts and CP-Ws are not dynamically coordinated for each other. We conduct ENSO ensemble forecasting experiments with CP-Ts and CP-Ws as initial perturbations, where CP-Ts and CP-Ws possess the same amplitudes as those of the corresponding components of C-CNOPs. The results reveal that CP-Ts and CP-Ws ensemble mean forecasts can capture realistic El Niño and La Niña events at a lead time of 9 months (see Figure 2). However, they yield larger forecast errors than the CP-ensemble mean forecast when forecasting the Niño3.4 SSTA during the mature phase, with the highest deviation occurring at lead times of 6 and 9 months (see Figure 3c).

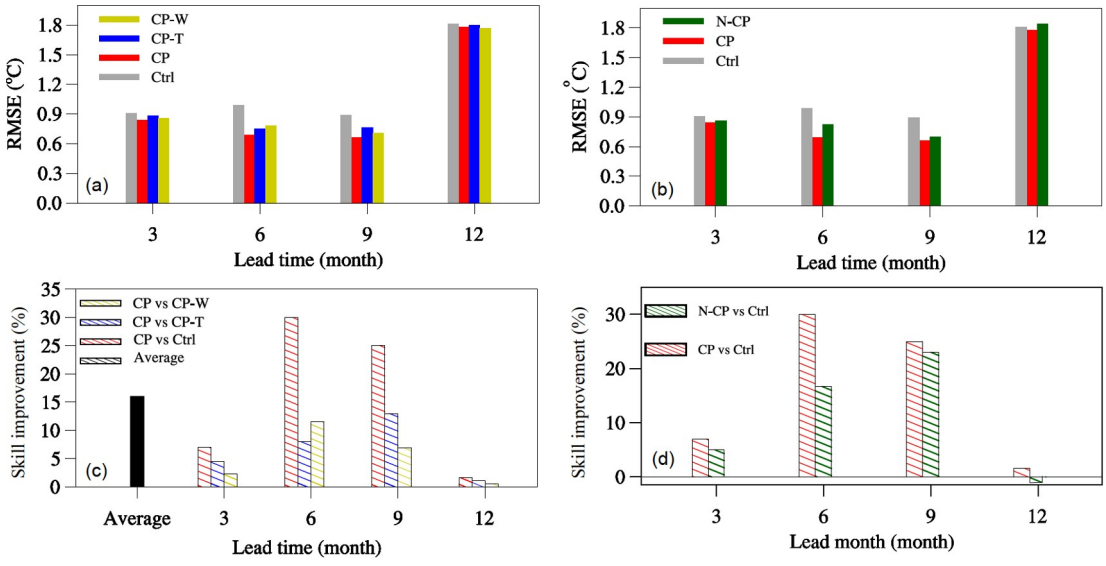

Figure 3 Predictions of the Niño3.4 SSTAs during the ENSO mature phase. (a) RMSE of the control forecasts and the CP, CP-T and CP-W ensemble mean forecasts; (b) RMSE of the control forecasts and the CP and N-CP ensemble mean forecasts; (c) the reduction degree of the RMSE (i.e., Skill Improvement in figures) for the CP-ensemble mean forecasts relative to the control forecasts averaged for all lead times, for the CP-ensemble mean forecasts relative to the control forecasts and the CP-T and CP-W ensemble mean forecasts at the lead times of 3, 6, 9, and 12 months; and (d) the reduction degree of the RMSE for the CP and N-CP ensemble mean forecasts relative to the control forecasts.

Based on the above results, the CP-ensemble mean forecast for the Niño3.4 SSTAs during the ENSO mature phase, especially at lead times of 6 and 9 months, significantly reduces the forecast errors relative to the control forecasts and the CP-T and CP-W ensemble mean forecasts. In other words, when the Niño3.4 SSTA during the mature phase is predicted from spring and summer, the CP-ensemble mean forecast imposes the greatest effect on reducing the forecast uncertainty. In fact, the CP-ensemble mean forecasts also exhibit the smallest forecast errors for the Niño3.4 SSTA during the mature phase when forecasting from these seasons (Figure 3). The same conclusion is also statistically obtained when forecasting the SSTAs from 1982 to 2015 starting at different seasons with a 1-year lead time (Figure 4). That is, when predicting from spring and summer, the CP-ensemble mean forecast exhibits the greatest improvement and the smallest forecast errors relative to the control forecasts and the CP-T and CP-W ensemble mean forecasts.

Previous studies have indicated that the SSTA signals in spring and early summer are generally much weaker than those during the other seasons, and the strength of ocean-atmosphere coupling is weakest in these seasons (Webster, 1995); thus, the current coupled models are less likely to capture this weak coupling signal, potentially leading to the occurrence of large amounts of atmospheric and oceanic noise during these seasons (Webster and Yang, 1992; Webster, 1995; Hou et al., 2019). Furthermore, due to the strongest ocean-atmosphere coupling instability in the tropical Pacific in spring and summer (Wang and Fang, 1996), these noise errors can be rapidly amplified, resulting in significant forecasting uncertainty (Xue et al., 1994; Chen et al., 1995; Mu et al., 2007a; Mu et al., 2007b). However, the CP-ensemble mean forecasts exhibit much higher forecast skill than the control forecasts and the CP-T and CP-W ensemble mean forecasts when predicting from these seasons. This finding suggests that CPs are more appropriate than CP-Ts and CP-Ws in describing the uncertainties of the spring weakest ocean-atmosphere coupling strength.

3.3.2 *Anomaly correlation coefficient*

In the last section, the ability of CPs for improving the ENSO forecasting skill is measured from the perspective of Niño3.4 SSTA forecast errors, i.e., primarily considering the forecast uncertainties of the ENSO event intensity. In this section, the ensemble mean forecasting ability for the spatial variability of ENSO events is investigated, and the similarity between the forecasts and the observations is assessed by using anomaly correlation coefficients (ACCs).

Figure 5 shows the statistical mean of the ACC for spatial variability predictions of SSTAs during the mature phase of both El Niño and La Niña events from 1982 to 2015. Figure 6 shows the differences in the spatial ACC of mature-phase SSTAs between the ensemble mean forecasts (including CP, CP-T and CP-W) and the control forecasts, and between the CP-ensemble mean forecasts and CP-T and CP-W ensemble mean forecasts. The results show that the spatial ACCs are highest in the central-eastern tropical Pacific in both the control forecasts and the ensemble mean forecasts, but gradually decline with increasing lead times (Figure 5). Nevertheless, the CP, CP-T and CP-W ensemble mean forecasts still exhibit relatively large areas with the ACCs exceeding 0.6 in the tropical central-eastern Pacific at a lead

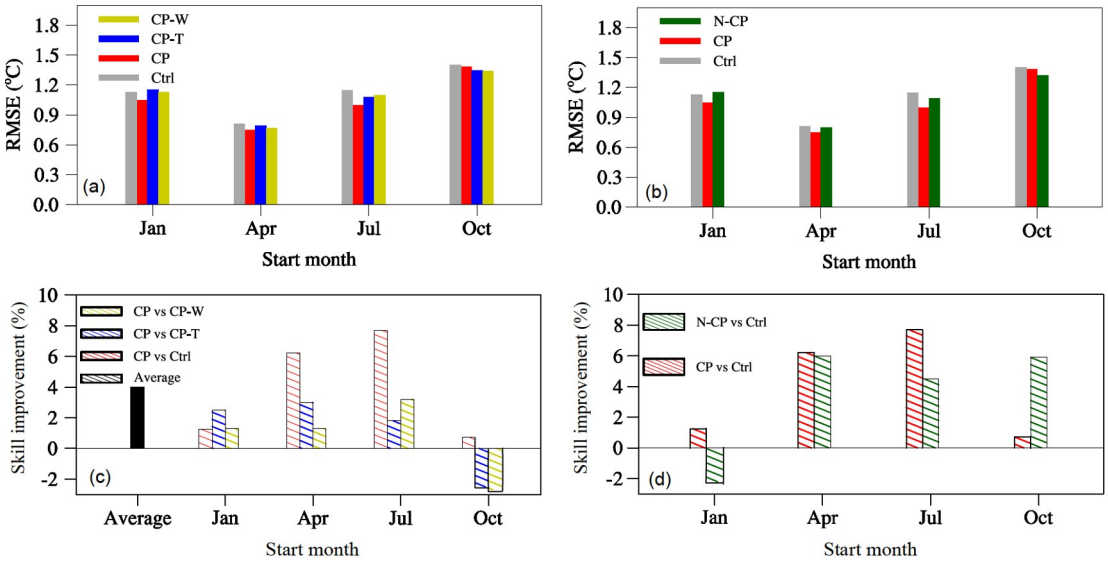

Figure 4 As in Figure 3, but for predictions of Niño3.4 SSTAs over the 1982–2015 period starting form January, April, July, and October, respectively. The lead time of predictions is one year.

time of 12 months; in contrast, the control forecasts exhibit an almost negligible ACC at this lead time. In other words, the above ensemble forecasts exhibit higher forecasting ability than the control forecasts for the spatial variability in the ENSO mature-phase SSTA. Much specifically, the CP-ensemble mean forecasts provide higher forecasting skill than the control forecasts in the equatorial southeast Pacific and tropical western Pacific; in particular, the CP-ensemble mean forecasts exhibit higher ACCs than the control forecasts and the CP-T and CP-W ensemble mean forecasts throughout the entire tropical Pacific region at a lead time of 12 months (see Figure 6).

In conclusion, the CP-ensemble mean forecasts, which incorporates the effect of initial ocean-atmosphere coupling uncertainties, are more favorable than the CP-T and CP-W ensemble mean forecasts for extending the lead times of skillful forecasts for the spatial variability of ENSO mature-phase SSTA, because of the lack of coupling ocean-atmosphere effects in the latter forecasts. Figure 5 indicates that the CP-ensemble mean forecast exhibits an ACC exceeding 0.6 in the tropical central-eastern Pacific for the ENSO mature-phase SSTA forecasts with a 12-month lead time. This result reveals that the CP-ensemble mean forecast successfully captures the signal of tropical central-eastern Pacific SSTA at a 12-month lead time, and statistically exhibits a higher forecast skill (based on the ACC) for ENSO mature-phase SSTA. Nevertheless, the forecasts of the Niño3.4 SSTA in Figure 2 shows that the CP-ensemble mean forecasts can capture major El Niño and La Niña events at a 9-month lead time, whereas at a 12-month lead time, despite the success of predicting most El Niño events (as depicted in Figure 2), it hardly captures La Niña events. In summary, the high ACC for predicting ENSO mature-phase SSTA at a 12-month lead time shown in Figure 5 is primarily reflected in the successful predictions of El Niño events; therefore, after comprehensive consideration of the forecast errors and the ACC, the CP-ensemble mean forecasts exhibit higher forecasting skill for El Niño mature-phase SSTA, with the useful forecasting skill extending beyond 12 months, while the useful forecasting skill for La Niña events is limited to 9 months.

3.4 Role of ocean-atmosphere coupling in initial perturbations for improving ENSO ensemble forecasting skill

The sea temperature and wind components of CPs are generated while considering their interactions, and they are dynamically coordinated (as shown in Figure 1). However, when CP-Ts and CP-Ws are combined to simultaneously perturb sea temperature and wind components of the control forecasts, although simultaneously considering initial uncertainties in the sea temperature and wind field, their interactions are not dynamically coordinated (for convenience, this type of perturbations are denoted as N-CPs; see Figure 1). What effect would the N-CP have on the forecasting skill if applied to ENSO ensemble forecasts? Answering this question could help reveal the role of the dynamical coupling of initial oceanic and atmospheric perturbations in improving the ENSO ensemble forecast skill.

We use the N-CP as the initial perturbations for ensemble forecasting and predict the SSTAs starting from January, April, July and October of each year with a lead time of 1 year. Similar to the CP-ensemble forecasts, 5 N-CPs are generated based on each control forecast. These N-CPs are subsequently added and subtracted from the initial analysis

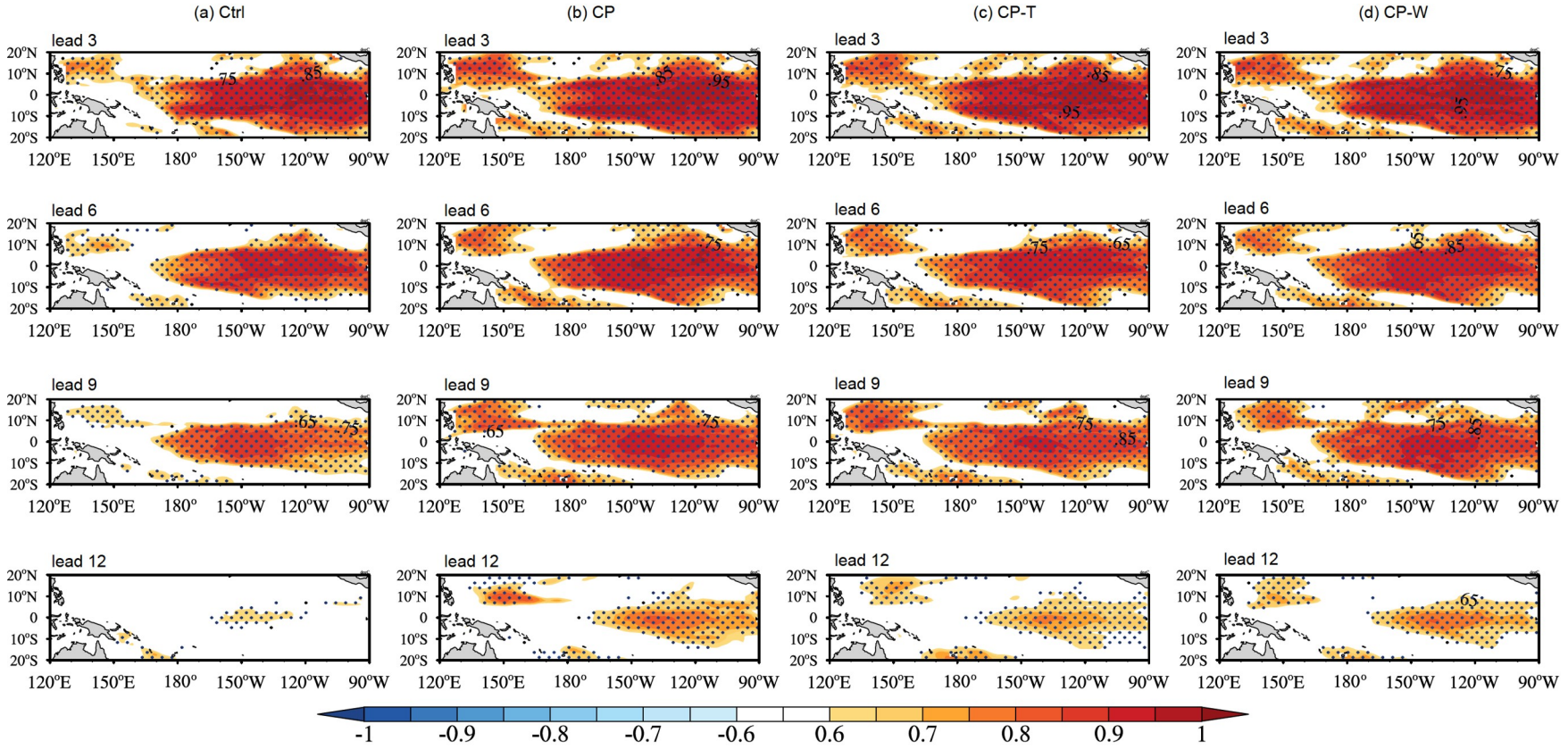

Figure 5 Spatial variability in the ACC of the predicted tropical Pacific SSTAs during the mature phase of El Niño and La Niña events from 1982 to 2015 at lead times of 3, 6, 9, and 12 months. (a) Control, (b) CP, (c) CP-T, and (d) CP-W. The dotted areas indicate significance at the 99% level.

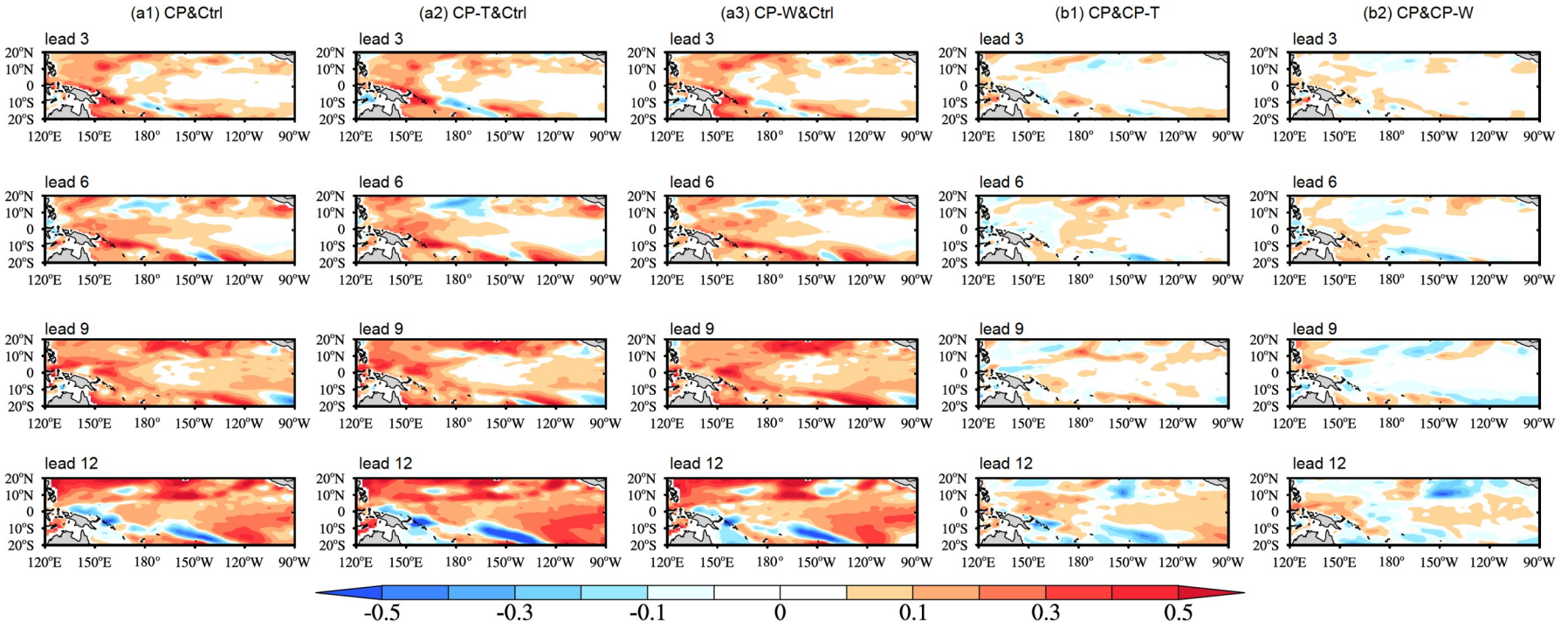

Figure 6 (a) Difference in the ACC of the mature-phase SSTAs for the CP, CP-T and CP-W ensemble mean forecasts compared with the control forecasts; (b) difference in the ACC of the mature-phase SST anomalies for the CP-ensemble mean forecast compared with the CP-T and CP-W ensemble mean forecasts.

field of the control forecast. Then, 10 perturbed forecasts are obtained, together with the control forecast, yielding a total of 11 ensemble members for each prediction. The N-CP ensemble mean forecast skill is compared to the CP-ensemble mean forecast skill to reveal the effect of initial coupling ocean-atmosphere uncertainties on improving the ENSO ensemble forecast skill.

Figure 3 shows the RMSE of the control forecasts and CP and N-CP ensemble mean forecasts for Niño3.4 SSTA during the ENSO mature phase, as well as the reductions of the prediction errors for CP and N-CP ensemble mean forecasts relative to the control forecasts. The results indicate, although both N-CP and CP-ensemble mean forecasts show much significant improvement relative to the control forecast at 6- and 9-month lead times, but the CP-ensemble mean forecasts show greater improvement. Specifically, at the lead time of 6 months, the improvement in the CP-ensemble mean forecasts relative to the control forecasts is approximately 13.3% greater than that in the N-CP ensemble mean forecasts. In other words, when forecasting the Niño3.4 SSTA during the ENSO mature phase from spring and summer, particularly from spring, the CP-ensemble mean forecasts obviously outperform the N-CP ensemble mean forecasts in terms of improving the control forecast skill. When forecasting monthly SSTA from 1982 to 2015 with the 12-month lead time starting from different seasons, the CP-ensemble mean forecast skill is often much higher than the N-CP ensemble mean forecast skill, even though the difference is not as significant as that for the forecasts of the mature phase Niño3.4 SSTA (Figure 4).

Regarding the prediction of the SSTA spatial variability during the ENSO mature phase, both CP and N-CP ensemble mean forecasts consistently exhibit higher ACCs than the control forecasts in the tropical Pacific at all lead times. Furthermore, when comparing CP and N-CP ensemble mean forecasts, the CP-ensemble mean forecast achieves a higher forecasting ability, especially in regions on both sides of the equator at longer lead times (Figures 7 and 8).

In summary, the CP-ensemble mean forecast achieves higher forecasting ability than the N-CP ensemble mean forecast for both the time series of Niño3.4 SSTAs and the SSTA spatial variability during the ENSO mature phase. Especially for forecasts starting in spring and summer, the CP-ensemble mean forecast provides more obvious advantages than the control and N-CP ensemble mean forecasts. Therefore, the CPs featured by dynamically-coordinated ocean-atmosphere interactions can extend the lead times of skillful ensemble mean forecasts for ENSO. Even though the ocean-atmosphere coupling strength is lowest in spring and summer, CPs can also successfully capture this subtle coupling signal, thereby effectively reducing the negative effect of the initial noise-induced forecast errors and significantly improving the forecast skill for ENSO.

3.5 Reliability of the CP-ensemble forecasts

Buizza et al. (2005) demonstrated that in a reliable ensemble forecasting system, the ensemble spread and RMSE of the ensemble mean forecast should be approximately equal. In fact, the closer their ratio is to 1, the more reliable the estimates of the prediction uncertainty provided by the ensemble forecasting system. Figure 9 shows the temporal variability in the ratio of the ensemble spread to the RMSE [i.e., RMSE/SPREAD; hereafter referred to as the reliability index (RI)] for CP, CP-T, CP-W and N-CP ensemble forecasts with respect to the Niño3.4 index. It is shown that although the RI of the CP-ensemble forecast does not reach approximately 1, it is much closer to 1 than those of the CP-T, CP-W and N-CP forecasts at all lead times. Therefore, the CP-ensemble forecast is more reliable than the CP-T, CP-W and N-CP ensemble forecasts, and the ensemble spread provides a better representation of the error of the ensemble mean forecasts for Niño3.4 SSTA in the tropical Pacific. Figure 10 shows the spatial distribution of the RIs for CP, CP-T, CP-W and N-CP ensemble forecasts in the tropical Pacific. As shown in the figure, the RIs for these ensemble forecasts are all approximately 1 in most areas north of the equator in the tropical central-eastern Pacific; however, in the tropical southeast Pacific, the RI significantly exceeds 1, approaching approximately 2. In any case, the RI of the CP-ensemble forecast always remains closer to 1 than those of the CP-T, CP-W and N-CP forecasts. Therefore, the spatial distribution of the RI also indicates that the CP-ensemble forecasts can better characterize the prediction uncertainties in the tropical central-eastern Pacific SSTA than the CP-T, CP-W and N-CP ensemble forecasts, especially accurately reflecting the prediction uncertainties of SSTA in the region north of the equator in the tropical central-eastern Pacific. Therefore, the CP-ensemble forecast provides higher reliability than the CP-T, CP-W, and N-CP ensemble forecasts, and yields more reliable estimates of the prediction uncertainties. In addition, Yang et al. (2012) demonstrated that current ensemble forecasts of climate often exhibit an overconfidence phenomenon in the ensemble and exhibit an ensemble spread significantly smaller than the RMSE of the ensemble mean forecast (also refer to Yang et al., 2016 and Liu et al., 2019). The above results indicate that dynamically coordinated coupled initial perturbations of oceanic and atmospheric variabilities could help increase the ensemble spread and reduce its distance from the RMSE of the ensemble mean forecast. This result suggests that the C-CNOP method is potential for yielding the fast-growing coupled initial perturbations that provide reliable members for ensemble forecasts of coupled system. More key variabilities in atmosphere and ocean could be contained in the C-CNOP for ENSO ensemble forecasting to enhance the RI much closer to 1.

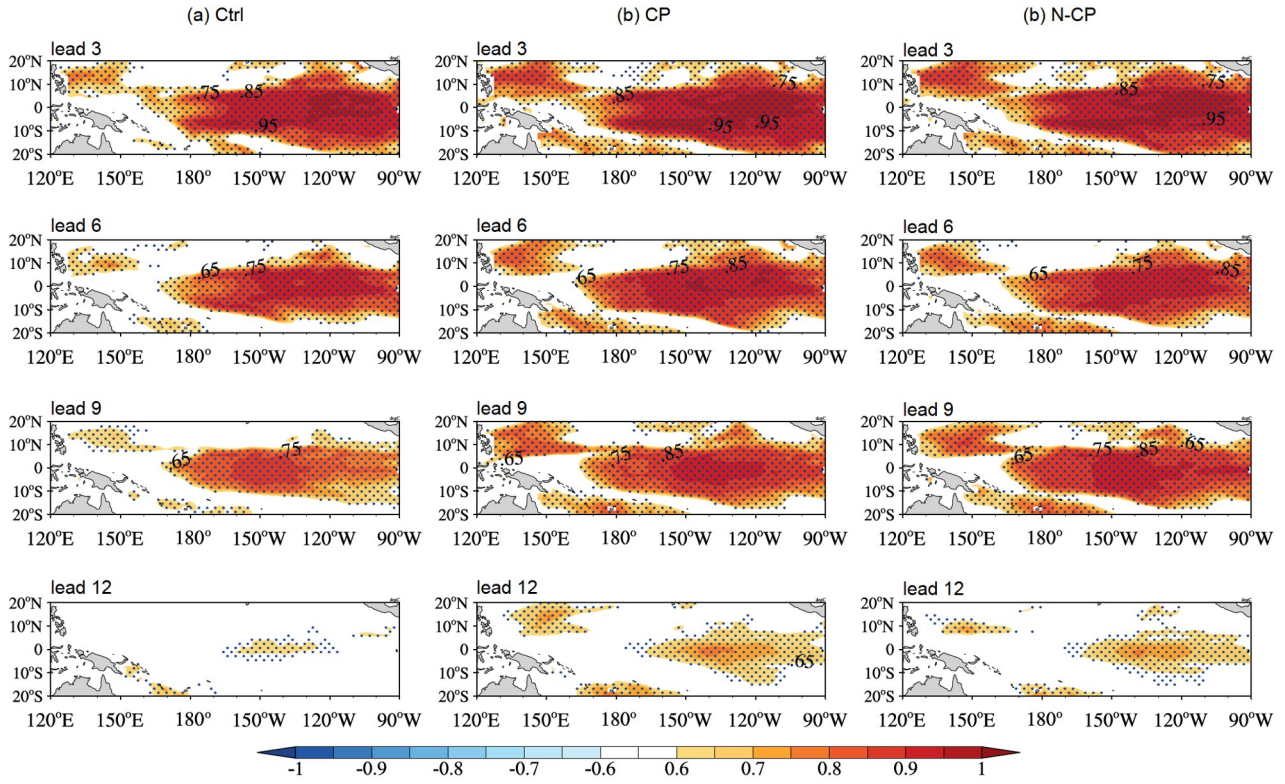

Figure 7 Spatial variability in the ACC of the predicted tropical Pacific SSTAs for the mature phases of El Niño and La Niña events from 1982–2015 at lead times of 3, 6, 9, and 12 months. (a) Control; (b) CP; (c) N-CP. The dotted areas indicate that the 99% significance test is passed.

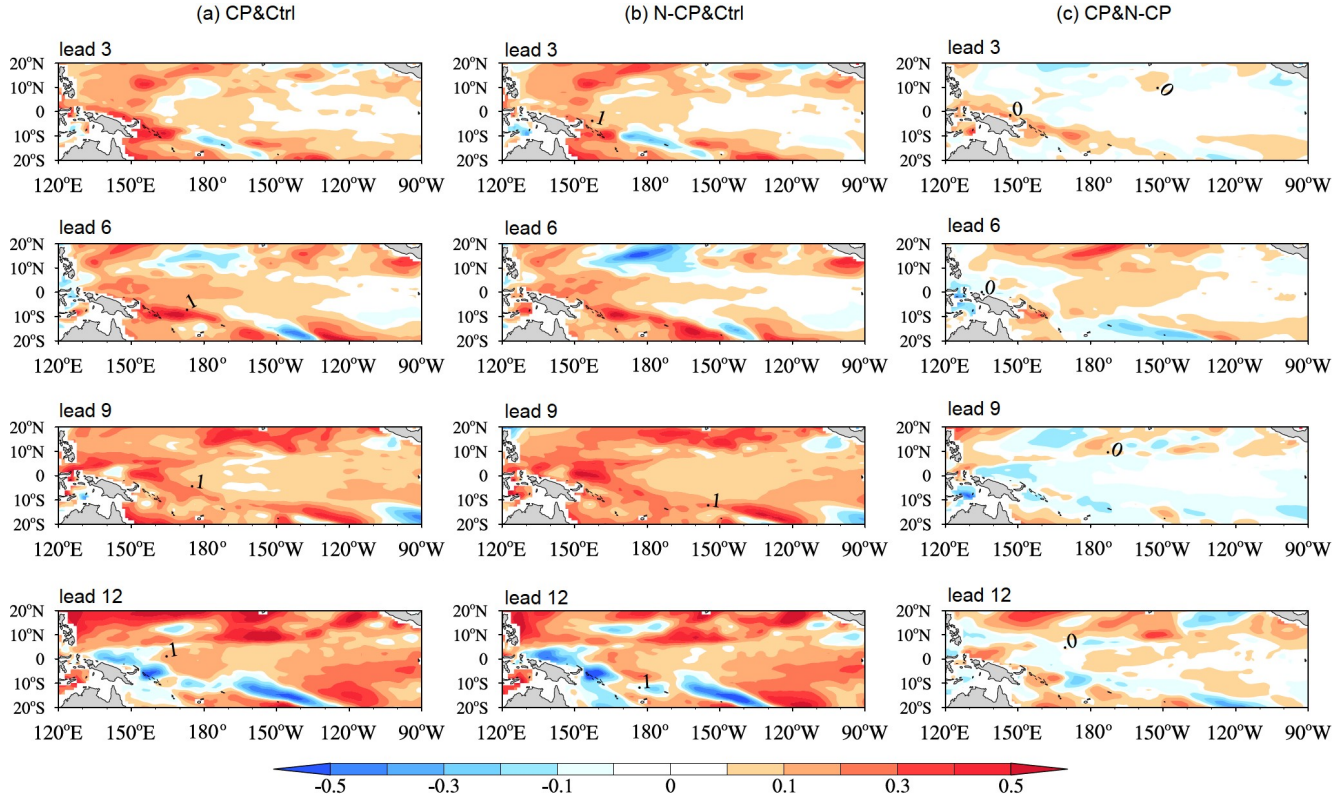

Figure 8 (a) Difference in the ACC for mature-phase SSTA of CP and N-CP ensemble mean forecasts relative to the control forecast; (b) difference in the ACC for mature-phase SSTA of the CP ensemble mean forecasts relative to the N-CP ensemble mean forecasts.

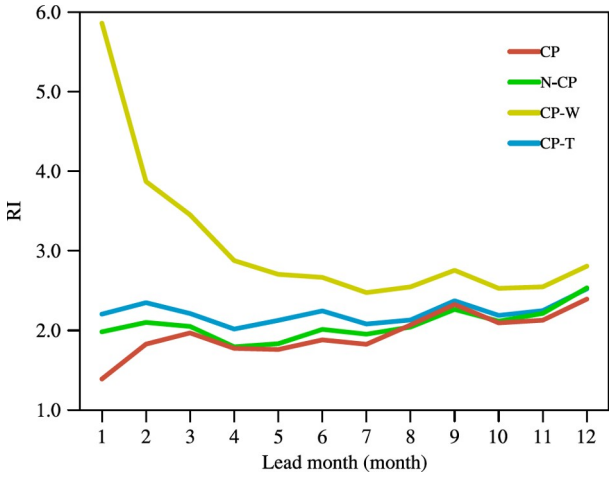

Figure 9 Temporal variability in the RI for CP (red), CP-T (blue), CP-W (yellow) and N-CP (green) ensemble forecasts.

4. Conclusion and discussion

The conventional initial perturbation methods for ensemble forecasting fail to effectively characterize the initial uncertainties arising from the interactions among the different components of the Earth system, which limits the skill improvement in ensemble forecasts with coupled models. To address this issue, the present study adopts directly the time series of the coupled model outputs to propose the coupled conditional nonlinear optimal perturbation (C-CNOP) method according to the nature of the solution of differential equations. The C-CNOP considers the coupling uncertainties of different spheres of the Earth system and represents the nonlinearly coupled fast-growing initial perturbation within the forecast period.

The C-CNOP method is used to generate the fast-growing coupled initial perturbations for the ensemble forecast of the Earth System Model CESM, and ensemble forecasting experiments are performed for ENSO events from 1982 to 2015. In this study, the importance of accounting for the effect of initial coupling uncertainty in improving the ENSO forecasting skill is revealed from both the temporal variability in Niño3.4 SSTA and the spatial variability in ENSO mature-phase SSTA. Results reveal that the ensemble mean forecast errors relative to the coupled initial perturbations (CPs) generated by the C-CNOP method are notably smaller than those of the control forecasts. In particular, the forecast errors of ENSO mature-phase SSTA predicted from spring and summer can be reduced by 30%. In addition, the CP-ensemble mean forecasts exhibit smaller forecast errors for ENSO mature-phase SSTA than the ensemble mean forecasts when perturbing the ocean temperature (CP-T) and atmosphere wind field (CP-W) separately. Furthermore, the

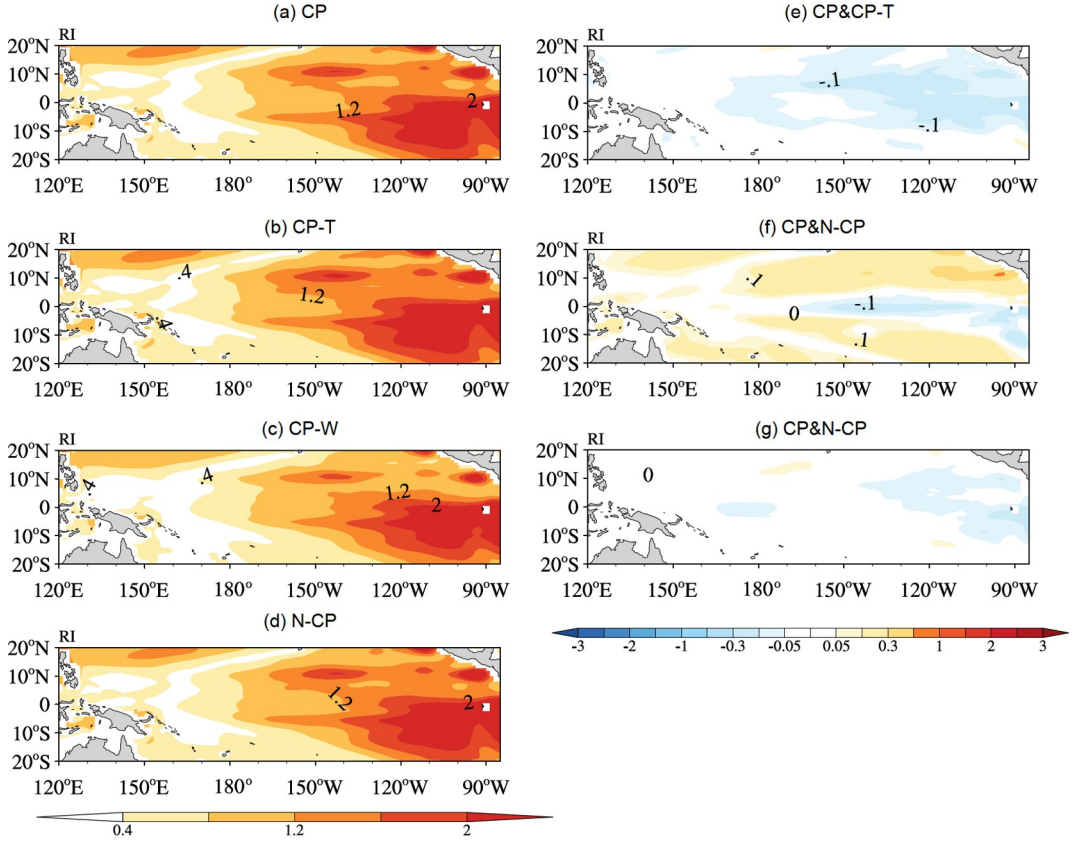

Figure 10 (a)–(d) Spatial distribution of RI for the CP, CP-T, CP-W and N-CP ensemble forecasts, and (e)–(g) differences of RI between CP and CP-T, CP-W, and N-CP, respectively.

greatest reduction in the forecast errors is observed in the forecasts starting from spring and summer. Physically, the tropical Pacific exhibits the lowest ocean-atmosphere coupling intensity in spring and early summer, which makes coupled model initialization more challenging for accurately capturing the subtle ocean-atmosphere interactions during this season, easily resulting in atmospheric and oceanic noise. Moreover, the noise errors are more likely to be rapidly amplified due to the high ocean-atmosphere coupling instability in this season, resulting in significant ENSO forecast uncertainties. However, the CPs can better describe the uncertainty in the weak ocean-atmosphere coupling in this season than CP-Ts with only initial sea temperature perturbations considered and CP-Ws with only wind perturbations considered. This performance of CPs further suppresses the rapid growth of prediction errors and provides a higher forecast skill than the CP-Ts and CP-Ws. Furthermore, the results show that the CP-ensemble mean forecast is more conducive to prolong the lead time of the skillful forecast measured by anomaly correlation coefficients (ACC) for the spatial variability in ENSO mature-phase SSTA than the CP-T and CP-W ensemble mean forecasts. Therefore, in terms of both the forecast errors of Niño3.4 SSTA and the ACC of the spatial variability in ENSO mature-phase SSTA, the skill of the CP-ensemble mean forecast is significantly higher than those of the control forecasts and the CP-T and CP-W ensemble mean forecasts. As a result, incorporating initial ocean-atmosphere coupling uncertainty in ensemble initial perturbations is crucial for improving the ENSO forecast skill, especially for predictions starting from spring and summer.

In addition, in this study, CP-T and CP-W are simply combined to form a combination model of sea temperature and wind field perturbations (i.e., N-CP), and ENSO ensemble forecasting experiments are conducted including a comparison of the results with those of the CP-ensemble mean forecasts. The results show that the CP-ensemble mean forecasts can more obviously improve the forecast skill of the control forecasts than the N-CP ensemble mean forecasts, especially for predictions starting from spring and summer. The CP-ensemble mean forecasts yield a higher ACC for the spatial variability in ENSO mature-phase SSTA than the N-CP ensemble mean forecasts, and this advantage is particularly evident for SSTA forecasts on both sides of the equator with longer lead times. Therefore, CPs that appropriately incorporate the dynamically coordinated interactions of oceanic and atmospheric uncertainties can effectively increase the lead time of skillful forecasts for ENSO events; especially, CPs can capture the weak ocean-atmosphere coupling signals in spring and summer, thus largely reducing the forecast errors caused by arbitrary amplification of the initial noise during this season.

A reliability assessment of the CP-ensemble forecasts is also conducted in this study. The results indicate that the CP-ensemble forecasts better capture the consistency relationship between the ensemble mean forecast error and ensemble spread than the CP-T, CP-W and N-CP ensemble forecasts from both temporal and spatial variability perspectives, especially in the area north of the equator in the tropical central-eastern Pacific. Therefore, for ENSO prediction, CP-ensemble forecasts that more appropriately account for ocean-atmosphere coupling uncertainty can provide better estimates of the prediction uncertainty than CP-T, CP-W and N-CP ensemble forecasts, indicating that the CPs generated by the C-CNOP method are helpful for overcoming the overconfidence phenomenon in existing ensemble forecasts for climate.

In summary, CPs generated by the C-CNOP method better considers initial ocean–atmosphere coupling uncertainties, resulting in higher ensemble mean forecasting skill for ENSO. In particular, the forecasts of ENSO mature-phase SSTA with higher forecasting skills starting in spring and summer further highlights the superior performance of C-CNOPs in capturing the initial ocean-atmosphere coupling uncertainty. However, it should be noted that the above conclusions are mainly based on ensemble mean forecast results, which mainly focus on the role of the C-CNOP method in improving the deterministic forecast skill of ensemble forecasting. These satisfactory results encourage us to further investigate the role of C-CNOPs in improving the probabilistic forecast ability of ensemble forecasting by utilizing more ENSO events or longer time series. Additionally, to quickly demonstrate the dynamic rationality of the C-CNOP method and to reduce the computational burden of ensemble forecasts, we initially use a smaller number of perturbation samples in the ensemble forecast experiments. However, the C-CNOP method yields better ensemble forecasts than atmospheric or oceanic perturbations or simple combinations of these perturbations. Therefore, how many ensemble members should be used to achieve the highest ensemble forecasting skill when using the C-CNOP method in combination with the coupled model should be investigated in the future. Under this scenario, does the C-CNOP method provide more obvious advantages over other perturbation methods in improving the ensemble forecast skill? Do C-CNOPs exhibit a more reliable consistency relationship between the RMSE of the ensemble mean forecast and the ensemble spread? These questions must be further studied in the future. Furthermore, how to reasonably compare the C-CNOP method with the SV and BV methods without appropriately considering initial coupling uncertainties for different spheres of the Earth system should be considered. In conclusion, we hope to further develop the C-CNOP method to have much solid theoretical basis and the ability to achieve forecasting skill improvement, expecting that it plays important role in future weather-climate seamless predictions and even Earth System predictions.

Acknowledgements *The authors thank the two anonymous reviewers for their insightful comments and suggestions. The datasets generated and/or analyzed in this study are stored on computers at the State Key Laboratory of Numerical Modeling for Atmospheric Sciences and Geophysical Fluid Dynamics (LASG; https://www.lasg.ac.cn) and could be made available to researchers upon request. This work was supported by the National Natural Science Foundation of China (Grant Nos. 42330111 and 41930971).*

Conflict of interest The authors declare that there are no conflicts of interest.

References

Baehr J, Piontek R. 2014. Ensemble initialization of the oceanic component of a coupled model through bred vectors at seasonal-to-interannual timescales. Geosci Model Dev, 7: 453–461

Buizza R, Palmer T N. 1995. The singular-vector structure of the atmospheric global circulation. J Atmos Sci, 52: 1434–1456

Buizza R, Houtekamer P L, Pellerin G, Toth Z, Zhu Y, Wei M. 2005. A comparison of the ECMWF, MSC, and NCEP global ensemble prediction systems. Mon Weather Rev, 133: 1076–1097

Chen D, Zebiak S E, Busalacchi A J, Cane M A. 1995. An improved procedure for EI Niño forecasting: Implications for predictability. Science, 269: 1699–1702

Craig A P, Vertenstein M, Jacob R. 2012. A new flexible coupler for earth system modeling developed for CCSM4 and CESM1. Int J High Perform Comput Appl, 26: 31–42

Du H, Doblas-Reyes F J, García-Serrano J, Guemas V, Soufflet Y, Wouters B. 2012. Sensitivity of decadal predictions to the initial atmospheric and oceanic perturbations. Clim Dyn, 39: 2013–2023

Du J, Berner J, Buizza R, Charron M, Houtekamer P, Hou D, Jankov I, Mu M, Wang X G, Wei M Z, Yuan H L. 2018. Ensemble Methods for Meteorological Predictions. Handbook of Hydrometeorological Ensemble Forecasting. Spring. 1–52

Du J, Zhou B, Levit J. 2019. Measure of forecast challenge and predictability horizon diagram index for ensemble models. Weather Forecast, 34: 603–615

Duan W, Liu X, Zhu K, Mu M. 2009. Exploring the initial errors that cause a significant “spring predictability barrier” for El Niño events. J Geophys Res, 114: 2008JC004925

Duan W, Wei C. 2013. The ‘spring predictability barrier’ for ENSO predictions and its possible mechanism: Results from a fully coupled model. Intl J Clim, 33: 1280–1292

Duan W, Huo Z. 2016. An approach to generating mutually independent initial perturbations for ensemble forecasts: Orthogonal conditional nonlinear optimal perturbations. J Atmos Sci, 73: 997–1014

Duan W S, Mu M. 2018. Predictability of El Niño-Southern Oscillation Events. Oxford Research Encyclopedia of Climate Science

Duan W, Feng R, Yang C, Jiang L. 2022. A new approach to data assimilation for numerical weather forecasting and climate prediction. J Appl Anal Comput, 12: 1007–1021

Duan W, Yang L, Mu M, Wang B, Shen X, Meng Z, Ding R. 2023a. Recent advances in China on the predictability of weather and climate. Adv Atmos Sci, 40: 1521–1547

Duan W S, Yang L C, Xu Z Z, Chen J. 2023b. Conditional nonlinear optimal perturbation: Applications to ensemble forecasting of high-impact weather systems. In: Seon Ki Park, ed. Numerical Weather Prediction: East Asian Perspectives. Springer Atmos Sci, 17: 441–460

Hou M, Duan W, Zhi X. 2019. Season-dependent predictability barrier for two types of El Niño revealed by an approach to data analysis for predictability. Clim Dyn, 53: 5561–5581

Hunke E C, Lipscomb W H, Turner A K, Jeffery N, Elliott S. 2008. The Los Alamos sea ice model documentation and software users manual. Version 4.0. Los Alamos National Laboratory

Huo Z, Duan W. 2018. The application of the orthogonal conditional nonlinear optimal perturbations method to typhoon track ensemble forecasts. Sci China Earth Sci, 62: 376–388

Huo Z, Duan W, Zhou F. 2019. Ensemble forecasts of tropical cyclone track with orthogonal conditional nonlinear optimal perturbations. Adv Atmos Sci, 36: 231–247

Kleeman R, Tang Y, Moore A M. 2003. The calculation of climatically relevant singular vectors in the presence of weather noise as applied to the ENSO problem. J Atmos Sci, 60: 2856–2868

Lian T, Wang J, Chen D, Liu T, Wang D. 2023. A strong 2023/24 El Niño is staged by Tropical Pacific Ocean heat content buildup. Ocean-Land-Atmos Res, 2: 0011

Liu T, Tang Y, Yang D, Cheng Y, Song X, Hou Z, Shen Z, Gao Y, Wu Y, Li X, Zhang B. 2019. The relationship among probabilistic, deterministic and potential skills in predicting the ENSO for the past 161 years. Clim Dyn, 53: 6947–6960

Molteni F, Buizza R, Palmer T N, Petroliagis T. 1996. The ECMWF ensemble prediction system: Methodology and validation. Quart J R Meteoro Soc, 122: 73–119

Mu M, Duan W S, Wang B. 2003. Conditional nonlinear optimal perturbation and its applications. Nonlin Process Geophys, 10: 493–501

Mu M, Xu H, Duan W. 2007a. A kind of initial errors related to “spring predictability barrier” for El Niño events in Zebiak-Cane model. Geophys Res Lett, 34: 2006GL027412

Mu M, Duan W, Wang B. 2007b. Season-dependent dynamics of nonlinear optimal error growth and El Niño-Southern Oscillation predictability in a theoretical model. J Geophys Res, 112: 2005JD006981

Mureau R, Molteni F, Palmer T N. 1993. Ensemble prediction using dynamically conditioned perturbations. Quart J R Meteoro Soc, 119: 299–323

Neale R B, Richter J H, Conley A J, Park S, Lauritzen P H, Gettelman A, Williamson D L, Rasch P J,Vavrus S J,Taylor M A, Collins W D, Zhang M H, Lin S J. 2010. Description of the NCAR Community Atmosphere Model (CAM5. 0). Technical Report. Note NCAR/TN-486+ STR, 1: 1–12

Oleson K W, Lawrence D M, Bonan G B, Flanner M G, Kluzek E, Lawrence P J, Levis S, Swenson S C, Thornton P E, Dai A, Decker M, Dickinson R, Feddema J, Heald C L, Hoffman F, Lamarque J F, Mahowald N, Niu G Y, Qian T, Randerson J, Running S, Sakaguchi K, Slater A, Stöckli R, Wang A, Yang Z, Zeng X D, Zeng X B. 2010. Technical description of version 4.0 of the Community Land Model (CLM). Technical Report. National Center for Atmospheric Research

Smith R, Jones P, Briegleb B, Bryan F, Danabasoglu G, Dennis J, Dukowicz J, Eden C, Fox-Kemper B, Gent P, Hecht M, Jayne S, Jochum M, Large W, Lindsay K, Maltrud M, Norton N, Peacock S, Vertenstein M, Yeager S. 2010. The parallel ocean program (POP) reference manual ocean component of the community climate system model (CCSM) and community earth system model (CESM). LAUR-01853, 141: 1–140

Tang Y, Zhang R H, Liu T, Duan W, Yang D, Zheng F, Ren H, Lian T, Gao C, Chen D, Mu M. 2018. Progress in ENSO prediction and predictability study. Natl Sci Rev, 5: 826–839

Toth Z, Kalnay E. 1993. Ensemble forecasting at NMC: The generation of perturbations. Bull Amer Meteor Soc, 74: 2317–2330

Vannitsem S, Duan W. 2020. On the use of near-neutral Backward Lyapunov Vectors to get reliable ensemble forecasts in coupled ocean-atmosphere systems. Clim Dyn, 55: 1125–1139

Wang B, Fang Z. 1996. Chaotic oscillations of tropical climate: A dynamic system theory for ENSO. J Atmos Sci, 53: 2786–2802

Webster P J, Yang S. 1992. Monsoon and Enso: Selectively interactive systems. Quart J R Meteoro Soc, 118: 877–926

Webster P J. 1995. The annual cycle and the predictability of the tropical coupled ocean-atmosphere system. Meteorl Atmos Phys, 56: 33–55

Xie S P, Philander S G H. 1994. A coupled ocean-atmosphere model of

relevance to the ITCZ in the eastern Pacific. Tellus A-Dynam Meteor Oceanogr, 46: 340–350
Xue Y, Cane M A, Zebiak S E, Blumenthal M B. 1994. On the prediction of ENSO: A study with a low-order Markov model. Tellus A-Dynam Meteor Oceanogr, 46: 512–528
Yan L, Yu Y, Wang B, Li L, Wang P. 2009. ENSO hindcast experiments using a coupled GCM. Atmos Ocean Sci Lett, 2: 7–13
Yang D, Tang Y, Zhang Y, Yang X. 2012. Information-based potential predictability of the Asian summer monsoon in a coupled model. J Geophys Res, 117: 2011JD016775
Yang D, Yang X, Xie Q, Zhang Y, Ren X, Tang Y. 2016. Probabilistic versus deterministic skill in predicting the western North Pacific-East Asian summer monsoon variability with multimodel ensembles. J Geophys Res-Atmos, 121: 1079–1103
Zhang H, Duan W, Zhang Y. 2023. Using the orthogonal conditional nonlinear optimal perturbations approach to address the uncertainties of tropical cyclone track forecasts generated by the WRF model. Weather Forecast, 38: 1907–1933
Zheng F, Zhu J. 2010. Coupled assimilation for an intermediated coupled ENSO prediction model. Ocean Dyn, 60: 1061–1073

(Editorial handling: Lili LEI)

中国科学: 地球科学 2024 年 第 54 卷 第 3 期: 845 ~ 861
SCIENTIA SINICA Terrae earthcn.scichina.com
《中国科学》杂志社 SCIENCE CHINA PRESS
论 文

耦合条件非线性最优扰动及其在ENSO集合预报研究中的应用

段晚锁[1,2*], 胡蕾[1,2], 冯蓉[1]

1. 中国科学院大气物理研究所大气科学和地球流体力学数值模拟国家重点实验室, 北京 100029;
2. 中国科学院大学, 北京 100049
* 通讯作者, E-mail: duanws@lasg.iap.ac.cn

收稿日期: 2023-08-04; 收修改稿日期: 2024-01-27; 接受日期: 2024-02-07; 网络版发表日期: 2024-02-26
国家自然科学基金项目(批准号: 42330111、41930971)资助

摘要 考虑到目前集合预报初始扰动方法未能充分刻画地球系统不同圈层相互作用影响的局限性, 本研究提出了能够考虑多圈层耦合初始不确定性的耦合条件非线性最优扰动(C-CNOP)方法. 将C-CNOP方法应用于热带太平洋典型的海气耦合现象厄尔尼诺-南方涛动(ENSO)事件的集合预报研究, 表明了C-CNOP方法能够产生ENSO集合预报的更恰当考虑海气耦合不确定性的快速增长初始扰动(CPs); 从Niño3.4海表温度距平(SSTA)时间变率的预报和ENSO成熟位相SSTA空间变率的预报两方面, 揭示了CPs能够有效促进ENSO集合平均预报的水平, 尤其从春、夏季开始的预报, 即使该季节热带太平洋海气耦合强度最弱, CPs也能够捕捉到该弱海气耦合信息的不确定性, 从而大大抑制了ENSO预报误差在该季节由于最强海气耦合不稳定性导致的快速增长, 有效延长了ENSO的预报时效. 因此, C-CNOP方法是一个能够产生集合预报的更充分考虑初始耦合不确定性的初始扰动的方法, 期望未来在继续研究的基础上, 使C-CNOP在地球气候系统预测中发挥重要作用.

关键词 集合预报, 多圈层相互作用, 初始扰动, ENSO

1 引言

集合预报是估计天气气候预报结果不确定性, 提高数值预报水平的重要手段, 已被世界气象组织列为未来数值预报的主要发展战略之一. 集合预报质量的高低取决于如何产生初始扰动样本(Du等, 2018). 已有研究表明, 只有在控制预报上叠加增长型初始扰动才有助于集合预报达到更高水平(Toth和Kalnay, 1993; Duan等, 2023a, 2023b), 而对于需要考虑地球系统多圈层相互作用的气候变率的预测, 该类增长型初始扰动还须能够反映不同圈层耦合过程的不确定性, 才能使地球气候系统的预测水平进一步提高. 目前国际上主流的增长型初始扰动方法有繁殖向量法(BVs; Toth和Kalnay, 1993)和奇异向量法(SVs; Mureau等, 1993; Buizza和Palmer, 1995). BVs方法已于1992年被应用于美国国家环境预报中心(NCEP)的集合预报系统, 而欧洲数值天气预报中心(ECMWF)在1992年将SVs方法应用于集合预报, 并且在数值天气预报中取得了巨大成

中文引用格式: 段晚锁, 胡蕾, 冯蓉. 2024. 耦合条件非线性最优扰动及其在ENSO集合预报研究中的应用. 中国科学: 地球科学, 54(3): 845–861, doi: 10.1360/SSTe-2023-0180
英文引用格式: Duan W, Hu L, Feng R. 2024. Coupled conditional nonlinear optimal perturbations and their application to ENSO ensemble forecasts. Science China Earth Sciences, 67(3): 826–842, https://doi.org/10.1007/s11430-023-1273-1

功. SVs至今仍是ECMWF集合预报的基本方法之一(https://confluence.ecmwf.int/display/FUG/). BVs和SVs方法各有优势, 但它们产生的初始扰动均不能很好地表征不同圈层耦合过程的初始不确定性(Kleeman等, 2003; Vannitsem和Duan, 2020). 耦合系统的BVs, 一般是在预报起始时间之前通过繁殖包含不同变率的初始扰动来产生, 但这样得到的增长型初始扰动不能保证其在预报时间段的快速增长行为(Du等, 2019; Duan等, 2023a), 从而导致BVs仅能使集合预报在较短的预报时间内获得有用的预报技巧(Zhang等, 2023). Vannitsem和Duan(2020)进一步将不依赖于繁殖参数的向后李雅普诺夫向量(Backward Lyapunov Vectors, 简称BLVs)方法应用于低阶多尺度海气耦合模式的集合预报, 表明增长最快的BLVs描述快变的大气不确定性, 而增长缓慢或不增长的BLVs模态则主要刻画慢变的海洋不确定性. 因此, 如果按照集合预报要求采用快速增长的初始扰动作为集合初始扰动样本, 那么缓慢或不增长的初始扰动不利于集合预报达到更高预报技巧, 但BLVs快速增长扰动又主要体现大气的天气尺度变率, 不能反应海气变率耦合不确定性影响下的快速增长扰动, 从而不利于提高具有气候变率的海气耦合事件的集合预报水平. ECMWF的SVs方法刻画了预报时间段控制预报的(线性)快速增长扰动, 具有明确的动力学意义, 这可能是其在数值天气预报中取得巨大成功的主要原因之一(Du等, 2019; Duan等, 2023a, 2023b). 但不可否认, SVs基于线性模式获取, 不能充分反映非线性过程的影响(Mu等, 2003), 而且它在初始扰动中不能描述不同圈层特征变率耦合不确定性的影响(Kleeman等, 2003).

Duan和Huo(2016)考虑到SVs的线性局限性, 提出了正交条件非线性最优扰动(Orthogonal Conditional Nonlinear Optimal Perturbations, 简称O-CNOPs)集合预报新方法. O-CNOPs方法不仅考虑了非线性物理过程的影响, 而且刻画了预报时间段控制预报的快速增长初始扰动. 该方法已被应用于台风路径的集合预报研究, 不仅有效减小了台风路径的预报误差, 而且对台风的登陆地点, 登陆时间, 甚至台风路径的转向, 都较传统的SVs和BVs有更高的预报技巧(Huo和Duan, 2018; Huo等, 2019; Duan等, 2023a, 2023b; Zhang等, 2023). 然而, O-CNOPs与SVs方法类似, 将其应用于耦合模式时, 它无法刻画不同圈层耦合过程初始不确定性的影响. 鉴于O-CNOPs的局限性, 但同时考虑到它刻画预报时间段非线性增长初始扰动的优势, 该研究将在O-CNOPs的基础上, 发展能够考虑耦合过程初始不确定性影响的耦合模式集合预报初始扰动方法, 即耦合条件非线性最优初始扰动(记为C-CNOP)方法, 从而获得一个既能充分刻画初始误差非线性不稳定增长, 又能考虑耦合过程不确定性且动力学意义合理的集合预报初始扰动方法.

ENSO是具有最强年际变率信号的热带海气耦合现象, 它的发生往往导致我国乃至全球天气气候的异常, 造成严重的自然灾害, 已经引起各国政府和公众的普遍关注. 因此, 准确预测ENSO具有重要意义(Lian等, 2023). 但目前大家认可的ENSO预测水平仅为6个月, 而且预报误差仍然较大(Tang等, 2018; Duan等, 2022, 2023a). 所以, 延长ENSO预报时效, 提高ENSO预报技巧, 有利于各国政府提前更长时间制定防灾减灾措施和合理部署国家的社会和经济活动.

对于ENSO的预报, 许多研究通过单独扰动大气或海洋, 或者同时但分别产生大气和海洋初始场扰动的方式开展集合预报(Yan等, 2009; Duan和Wei, 2013; Du等, 2012; Baehr和Piontek, 2014), 但如上所述, 该类初始扰动不能充分反映或未能描述大气、海洋初始不确定性相互作用的影响. 那么, 如果在ENSO集合预报中恰当考虑海气耦合不确定性对初始扰动的影响, ENSO的预报水平是否会显著提高? 特别地, 已有研究表明, 热带太平洋春季海气耦合强度最弱, 而目前的数值模式又很难捕捉到该季节的弱海气耦合信息, 从而当耦合模式从春节开始预测ENSO时, 初始场不能很好地包含这种弱海气信息(Webster, 1995; Zheng和Zhu, 2010), 从而造成额外的预报不确定性. 针对这种情形, 我们自然会问, 如果ENSO集合预报初始扰动能够较好反应春季最弱海气耦合强度的不确定性, ENSO预测水平是否可以有效提高呢? 为回答上述问题, 本文将使用C-CNOP开展ENSO的集合预报研究, 探讨考虑初始耦合不确定性对ENSO集合预报技巧的影响.

2 耦合条件非线性最优扰动(C-CNOP)

气候变率是具有不同特征变率的大气、海洋、陆面等不同圈层相互作用的结果, 所以气候变率的数值预测须使用地球气候系统耦合模式, 但由于目前人们

认知水平的限制, 现有的耦合模式尚不能准确刻画不同圈层相互作用的机制, 从而导致气候预测仍存在大的不确定性. 因此, 对于耦合模式的集合预报, 在动力学上更合理的增长型初始扰动, 还须考虑不同圈层初始耦合不确定性, 才能使耦合模式集合预报水平达到更高水平. 那么, 如何产生能够恰当包含不同圈层耦合不确定性的集合预报初始扰动呢?

为回答上述问题, 我们将多圈层耦合模式动力系统抽象为包含快变量(如大气中的天气尺度变率)和慢变量(如海洋中的气候尺度变率)相互作用的概念模型, 即考虑以下非线性偏微分方程组:

$$\begin{cases}\dfrac{\partial X}{\partial t}=F(X,Y,t)+f_X,\\ \dfrac{\partial Y}{\partial t}=\dfrac{1}{\epsilon}G(X,Y,t)+f_Y,\\ U_0=(X|_{t=0}=X_0,\ \ Y|_{t=0}=Y_0),\Omega\times[0,T],\end{cases}\tag{1}$$

其中, X和Y分别表示慢和快变量, $U_0=(X_0,Y_0)$代表它们的初始状态, t是时间, 且$t\in[0,T]$, $T<+\infty$, F和G均为非线性泛函, f_X和f_Y分别表示慢变量的外强迫(如海洋变率的潮汐、海表热通量, 以及淡水通量等外强迫)和快变量的外强迫(如大气变率的太阳辐射、二氧化碳浓度、气溶胶等外强迫), 参数$\epsilon\ll 1$区分了方程(1)中慢变量X和快变量Y.

考虑对慢变量X(如气候系统中的海洋温度)的预报, 可将方程(1)中对应于慢变量的微分方程写为微分形式:

$$\mathrm{d}X=F(X,Y,t)\mathrm{d}t+f_X\,\mathrm{d}t.\tag{2}$$

假定f_X和f_Y均为定常外强迫(如国际耦合模式比较计划CMIP试验中的工业革命前外强迫), 即仅考虑快、慢变量内部变率变化的影响. 在时间区间$[t_a,t_b]$ $(t_a<t_b\leqslant T)$上积分方程(2)可得:

$$\begin{aligned}\int_{t_a}^{t_b}\mathrm{d}X&=\int_{t_a}^{t_b}F(X,Y,t)\mathrm{d}t+\int_{t_a}^{t_b}f_X\,\mathrm{d}t\\&=\int_{t_a}^{t_b}F(X,Y,t)\mathrm{d}t+f_X(t_b-t_a).\end{aligned}\tag{3}$$

因此, 未来时刻t_b对应的慢变状态的预报变量X_{t_b}可表示为

$$X_{t_b}=X_{t_a}+\int_{t_a}^{t_b}F(X,Y,t)\mathrm{d}t+f_X(t_b-t_a).\tag{4}$$

方程(4)中存在拟代入的Y_{t_b}, 即快变量Y在未来时刻t_b的值. 事实上, Y_{t_b}可通过与方程(4)类似的方程(5)推导获得:

$$Y_{t_b}=Y_{t_a}+\frac{1}{\epsilon}\int_{t_a}^{t_b}G(X,Y,t)\mathrm{d}t+f_Y(t_b-t_a).\tag{5}$$

为方便起见, 记方程(4)和(5)中的初始状态$U_{t_a}=(X_{t_a},Y_{t_a})$, 终止状态$U_{t_b}=(X_{t_b},Y_{t_b})$.

如果从一个耦合模式输出的资料时间序列中选取两个时间段$[t_{01},t_1]$和$[t_{02},t_2]$, 那么它们各自的初始状态为$U_{t_{01}}=(X_{t_{01}},Y_{t_{01}})$和$U_{t_{02}}=(X_{t_{02}},Y_{t_{02}})$, 而根据方程(4)和(5), 它们对应的慢变量的终止状态X_{t_1}和X_{t_2}可表示为

$$X_{t_1}=\int_{t_{01}}^{t_1}F\mathrm{d}t+X_{t_{01}}+f_X(t_1-t_{01}),\tag{6}$$

$$X_{t_2}=\int_{t_{02}}^{t_2}F\mathrm{d}t+X_{t_{02}}+f_X(t_2-t_{02}).\tag{7}$$

如果两个积分时间段长度相同, 则方程(7)–(6)可得:

$$X_{t_2}-X_{t_1}=X_{t_{02}}-X_{t_{01}}+\left(\int_{t_{02}}^{t_2}F\mathrm{d}t-\int_{t_{01}}^{t_1}F\mathrm{d}t\right).\tag{8}$$

将方程(8)写成与方程(6)和方程(7)相同的形式, 则

$$X_{t_2}-X_{t_1}=X_{t_{02}}-X_{t_{01}}+\int_{\Sigma}\left[F_{t_{02}}-F_{t_{01}}\right]\mathrm{d}t.\tag{9}$$

其中, $F_{t_{02}}$代表方程(7)中的F, 对应的积分区间Σ表示时间段$[t_{02},t_2]$, 而$F_{t_{01}}$表示方程(6)中的F, 对应的Σ代表时间段$[t_{01},t_1]$. 特别地, 在方程(9)中的$F_{t_{01}}$和$F_{t_{02}}$, 存在快变量在t_1和t_2拟代入的状态值, 即Y_{t_2}和Y_{t_1}, 该两个状态值可有由方程(5)计算得到.

由方程(8)和(9)可知, X_{t_1}和X_{t_2}之间的差别源于初始状态$U_{t_{01}}$和$U_{t_{02}}$的差别, 也就是说, 慢变量X和快变量Y各自初始状态的差别相互作用共同导致慢变量在未来时刻存在差别. 如果将$[t_{01},t_1]$时间段的资料序列作为"观测序列", 则$[t_{02},t_2]$的时间序列可作为$[t_{01},t_1]$时间序列的"预报序列", 且其在终止时刻的预报误差仅由$U_{t_{02}}$

和$U_{t_{01}}$的差别，即慢、快变量的初始误差($X_{t_{02}}-X_{t_{01}}$, $Y_{t_{02}}-Y_{t_{01}}$)所导致.

对于给定的时间序列，考虑能够导致最大预报误差的初始误差, 则可建立如下优化问题:

$$J(u_{i,n})=\mathrm{MAX}(1\leqslant n<N;i<N)\,\|X_{T_{i,n}}-X_{T_i}\|, \quad (10)$$

其中，$u_{i,n}=(x_{i,n},y_{i,n})$代表了基于第$i$个观测序列及其$n$个预测序列所获得的在预报时刻$T$，能够导致预报变量最大预报误差的初始误差；$n<N$代表了预测序列的个数，在模式资料中可以大量选取，从而保证预测序列的多样性和所得结果统计上的显著性. 因此，由方程(10)获得的初始误差$u_{i,n}$，是基于有限但可使所得结果统计上显著的预测序列样本数，而获得的包含慢、快变量协调相互作用影响的初始误差.

如引言所述, CNOP代表了满足一定约束条件, 且在预报时刻能够导致最大预报误差的初始误差(Mu等, 2003). 对于方程(10), 如果将上述预测序列的有限但可使所得结果统计上显著的预测序列样本作为约束条件，则方程(10)给出了统计最优且包含快、慢变量相互作用不确定性的耦合CNOP, 记为C-CNOP.

上述针对慢变量的预报定义了C-CNOP. 事实上, 针对快变量的预报, 我们可类似地定义C-CNOP, 而且根据研究需要，还可将其拓展到更一般的地球系统多圈层特征变率相互作用的情形, 从而可为天气-气候无缝隙预报提供一个考虑多圈层相互作用，且能有效提高预报水平的集合预报初始扰动新方法. 为简单起见, 这里不再赘述.

3 C-CNOP在ENSO集合预报研究中的应用

将C-CNOP方法应用于地球系统模式(The Community Earth System Model, 简称CESM), 探讨在集合预报初始扰动中恰当考虑海气耦合不确定性对ENSO事件预报水平的促进作用.

3.1 模式和资料

CESM模式是由美国国家大气研究中心(National Center for Atmospheric Research, 简称NCAR)开发的地球系统模式. CESM 模式是一个全耦合的地球系统模式, 包括海洋、大气、陆面、海冰、陆冰等模块. 该研究中CESM模式采用大气分量模式(the Community Atmosphere Model 5, 简称CAM5, Neale等, 2010)和海洋分量模式(Parallel Ocean Program version, 简称POP, Smith等, 2010), 前者采用有限体积动力框架, 垂直方向30层，水平分辨率0.9°×1.25°(经度×纬度)等距规则网格, 后者采用垂直方向60层, 从表层10m逐渐变化到深层250m，水平方向则采用具有3个极点的广义正交曲线网格, 其中北半球的极点有2个, 分别位于北美大陆和亚洲大陆, 而南半球采用普通的麦卡托网格, 南北半球的网格在赤道上光滑衔接，水平分辨率在赤道地区为1°×0.27°(经度×纬度). CESM也包含了海冰分量模式(Community Ice Code version 4, 简称CICE4, Hunke和Lipscomb, 2008), 陆面模式(Community Land Model version 4, 简称CLM4, Oleson等, 2010). CESM模式的分量模式通过耦合器CPL7耦合(Craig等, 2012).

该研究采用美国大气海洋局国家环境预报中心的全球海洋数据同化系统资料集(Global Ocean Data Assimilation System, 简称GODAS), 该数据集是目前应用最为广泛的海洋实时同化数据集. 我们将GODAS海温资料，通过Nudging的方法同化到CESM的海洋模式初始场, 其中同化的水平区域覆盖全球海洋, 垂直方向从次表层15m至深层400m, 同化时间为1980~2015年. 采用所获得的同化资料作为初始场，积分CESM可获得关于热带太平洋海温的预报. 为方便，以下称该预报为“控制预报”(在图中记为“Ctrl”).

3.2 用C-CNOP产生ENSO集合预报的耦合初始扰动

Duan等(2018)表明, ENSO事件(无论是El Niño, 还是La Niña)的最快增长初始误差的空间结构不依赖ENSO事件本身，但对预报的起始时间比较敏感(Mu等, 2007a; 2007b; Duan等, 2009; Hou等, 2019). 所以, 如果从相应预测起始时间产生的快速增长初始误差模态中，提取该起始时间集合预报的快速增长初始扰动相空间的基底，那么这些基底应能刻画该起始时间对ENSO预测具有较大影响的初始误差的主模态. 此时, 只需根据对应控制预报的初始分析误差的振幅特征, 即可将这些基底通过向量线性组合的代数方法，张成该起始时间集合预报的非线性耦合快速增长初始扰动相空间，并采用该空间中的扰动样本开展ENSO集合预报试验.

本节将通过产生不同ENSO事件的C-CNOPs，构

建集合预报增长型耦合初始扰动相空间的基底，进而产生ENSO集合预报的快速增长耦合初始扰动样本，并考察该耦合初始扰动对ENSO集合预报技巧的影响.

利用工业革命前定常外强迫场，积分CESM模式200模式年，用后150年资料产生C-CNOPs. 在该资料序列中选取10个典型的El Niño年作为“观测”序列. 对于每一个序列，将150年资料中其余149年资料序列作为该“观测”序列的149次“预报”. 由第2节可知, 这些预报的预报误差仅由初始误差导致. 采用目标函数$J(t)$度量海表温度的预报误差,

$$J(t)=\sqrt{\frac{1}{N}\sum_{(i,j)}\left[T^{p}_{(i,j)}(t)-T^{o}_{(i,j)}(t)\right]^{2}}, \tag{11}$$

其中，T^{p}代表“预报”的海温，T^{o}代表“观测”的海温，(i,j)代表热带太平洋区域(20°S~20°N, 120°E~80°W)的格点, N是该区域总格点数. 采用上述“观测”和“预报”，根据方程(9)计算每次“预报”的C-CNOP, 该C-CNOP覆盖全球海洋, 包含海洋、大气、陆面等各个分量, 代表了CESM中在统计上对热带太平洋海温预报不确定性具有最大影响的耦合初始扰动(见第2节).

ENSO预报试验从每年的1月、4月、7月和10月开始, 且预报12个月, 则上述相应的“预报”在每一个起始月, 可产生 1 个C-CNOP, 10次“观测”El Niño的预报可得到10个C-CNOPs. 在上述C-CNOPs的基础上，我们将其后的第2~5快速增长耦合初始扰动也作为增长型初始扰动进行考虑. 这样, 对每个预报起始月, 10次“观测”事件共计产生50个快速增长初始扰动，我们统称其为C-CNOPs.

该研究探讨海洋和大气的耦合初始扰动对ENSO集合预报技巧的影响. 基于以上每个起始月份得到的50个C-CNOPs，对其海温分量T_0和风场分量(U_0, V_0)进行联合经验正交函数(Empirical Orthogonal Function, 简称EOF)分解，得到前20个主模态，记为$E_i=(T_{0i}, U_{0i}, V_{0i})$ (i=1, 2, 3, ... , 20; 解释方差达到90%以上). 对这20个主模态进行线性组合，可得初始海温和风场的联合扰动CP = $(IT_0, IU_0, IV_0)=\mathrm{a}_1E_1+\mathrm{a}_2E_2+\ldots+\mathrm{a}_{20}E_{20}$，其中$\mathrm{a}_i$为常系数. 显然, CP是相应起始月份的能够反映海气相互作用影响且快速增长的全球海温和风场耦合初始扰动. 选取不同系数a_i, 即可获得不同的耦合初始扰动, 将这些扰动作为ENSO集合预报的扰动样本，显然考虑了初始海气耦合不确定性. 如上所述，CP的大小可根据预报起始月份的初始分析误差的振幅特征确定, 初始分析误差大小由L2范数度量.

该研究对1982年1月~2015年12月期间的ENSO事件开展集合预报试验. 因为C-CNOP是该研究提出的新集合预报初始扰动方法，且在ENSO集合预报中是初次尝试，所以我们对每次预报仅试验性地产生5个CPs来验证C-CNOP的合理性. 将5个CPs分别以正负扰动对的形式叠加在控制预报(见第3节)初始场，积分CESM获得10次扰动预报，该10次扰动预报与控制预报一起形成该次预报的11个集合样本. 此处, CPs在水平方向覆盖全球，在垂直方向包含海表以下17层海温, 深度可达165m，约为赤道太平洋温跃层底层深度，以及大气底边界以上19层风场, 高度达到200hPa, 约为赤道太平洋Walker环流顶部高度. 作为CPs的一个例子，图1给出了1982/1983 El Niño当年4月起报时控制预报的5个CPs. 从图1可以看出, 5个CPs各自呈现了不同海温和风场模态，但我们发现当热带太平洋呈现局地冷海温异常时，异常风场主要表现为辐散，而当局地海温呈现暖异常时, 对应风场表现为辐合. 根据风-蒸发-海温反馈机制(Wind-Evaporation-SST，简称WES，Xie和Philander，1994)，上述海温和风场的反馈特征表明了CPs中海温和风场的相互作用是动力协调的.

3.3　热带太平洋海表温度距平的集合预报

为考察考虑初始耦合不确定性对ENSO集合预报技巧的影响，本节采用上述CPs，以1982年1月至2015年12月期间每年1月、4月、7月和10月为预报起始月, 对热带海表温度距平(SSTA)开展集合预报试验. 预报时长为1年, 共计136次预测试验.

3.3.1　预报误差

图2给出了GODAS数据集的Niño3.4区SSTA(即Niño3.4指数)的时间序列，以及超前3、6、9、12个月集合平均预报的ENSO事件成熟位相的Niño3.4 SSTA. 结果表明, 无论是控制预报还是CP-集合平均预报，均能提前9个月预报出主要的El Niño和La Niña事件，而CP-集合平均预报的结果与观测更为接近. 对不同预报时长，以及1982~2015年期间所有ENSO事件成熟位相Niño3.4 SSTA的预报误差(即均方根误差: RMSE)进行统计可知, CP-集合平均预报的预报误差较控制预报减

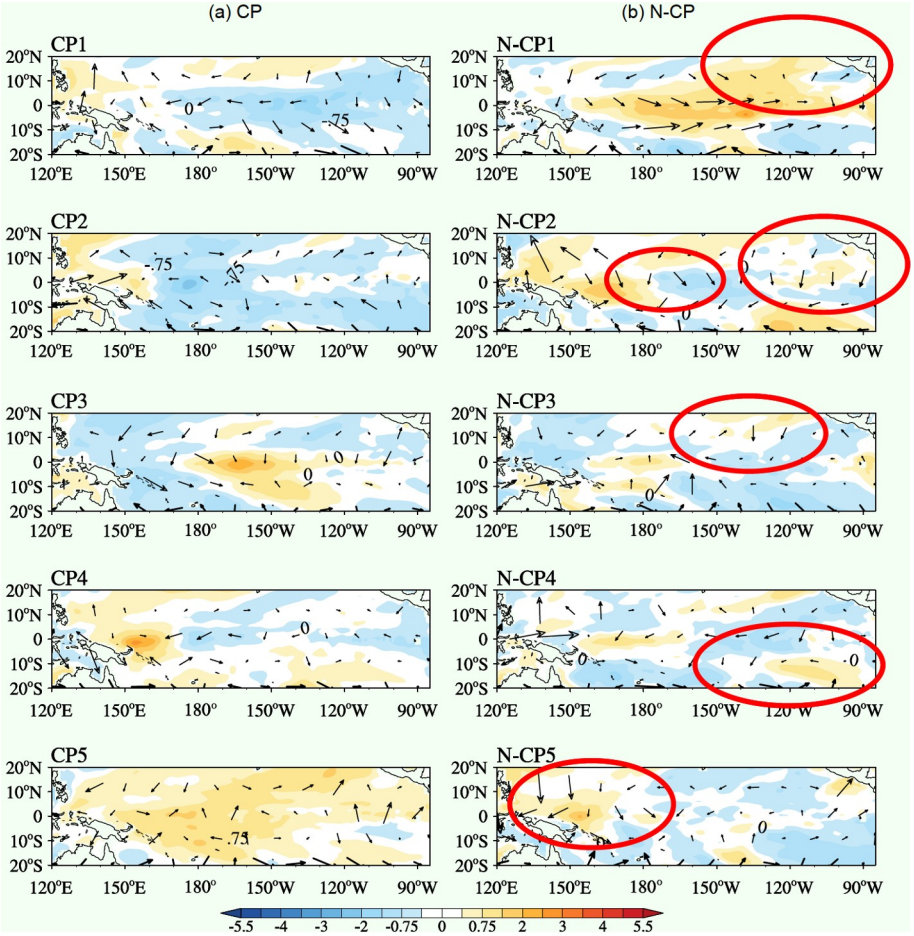

图 1　1982/1983 El Niño年4月起报时, 控制预报的5个CPs (a)和N-CPs (b)

阴影代表海表温度距平, 箭头代表风矢量

小约16%, 而对于超前预报时长为6个月的预报, CP-集合平均预报的预报误差较控制预报减小甚至高达30%, 在超前9个月也可达到25%.

为了考察ENSO集合预报初始扰动同时考虑海温和风场不确定性的重要性, 我们分别单独扰动海温和风场进行了集合预报试验. 为使海温和风场扰动在单独扰动情形下能够更好地描述他们各自的初始不确定性, 分别对C-CNOPs的海温和风场分量进行了EOF分解, 取前20个EOF海温主模态和前20个纬向风与经向风联合EOF主模态, 作为集合预报快速增长型初始扰动的基底. 利用这些基底, 分别产生集合预报初始海温扰动和风场扰动, 记为CP-T和CP-W. 图1给出了1982/83 El Niño当年4月起报时控制预报的5个CP-Ts和5个CP-Ws. 由图可以看出, CP-Ts和 CP-Ws与CPs的海温和风场分量具有不同的扰动分布, 且它们未能考虑海气相互作用的动力协调性. 我们分别以CP-Ts和-Ws为初始扰动, 开展ENSO集合预报试验. 此处, CP-Ts和-Ws具有与C-CNOPs对应分量相同的大小. 结果发现, CP-Ts和-Ws集合平均预报在超前9个月时捕捉到了主要的El Niño和La Niña事件(见图2), 但对成熟位相Niño3.4 SSTA的预报, 它们较CP-集合平均有更大的预报误差, 且在超前6个月和9个月预报时, 该偏差达到最大(见图3c).

由上述可知, CP-集合平均预报对ENSO成熟位相Niño3.4 SSTA的预报, 尤其在超前预报时长为6个月和9个月时, 较控制预报和CP-T和-W集合平均预报误差明显减小, 也就是说, 从春、夏季开始预报ENSO成熟位相Niño3.4 SSTA时, CP集合平均减小预报结果不确定性的效果最明显. 事实上, CP-集合平均预报在该季节起报时, 对成熟位相Niño3.4 SSTA预报的预报误差

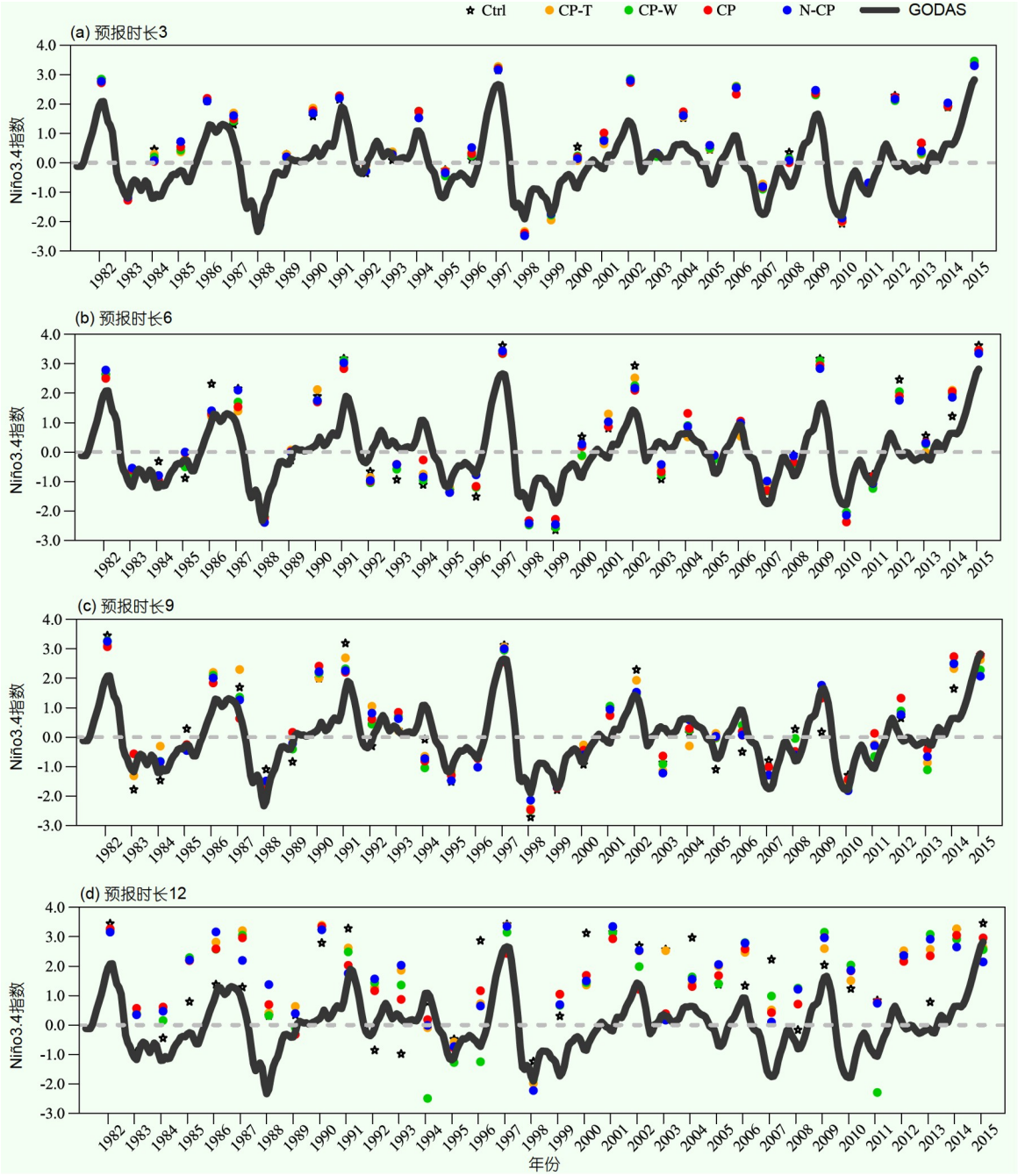

图 2　1982~2015年期间观测的Niño3.4区SSTA, 以及超前3个月(a)、6个月(b)、9个月(c)、12个月(d)对ENSO事件成熟位相Niño3.4指数的预报

黑线代表观测, 红、蓝、绿和黄点分别代表CP、N-CP、CP-T和CP-W集合平均预报, 星号代表控制预报

也是最小的(图3). 对于1982~2015年期间的SSTA, 分别从不同季节开始预报1年时, 统计上也获得了上述结论(图4). 已有研究表明, 在春季和夏初, 海温异常信号通常较其他季节更小, 海气耦合强度最弱(Webster, 1995), 耦合模式不易捕捉到该季节的弱耦合信号, 从而容易产生大气、海洋噪音(Webster和Yang, 1992; Webster, 1995; Hou等, 2019), 而且由于热带太平洋春夏季最强海气耦合不稳定性的影响(Wang和Fang,

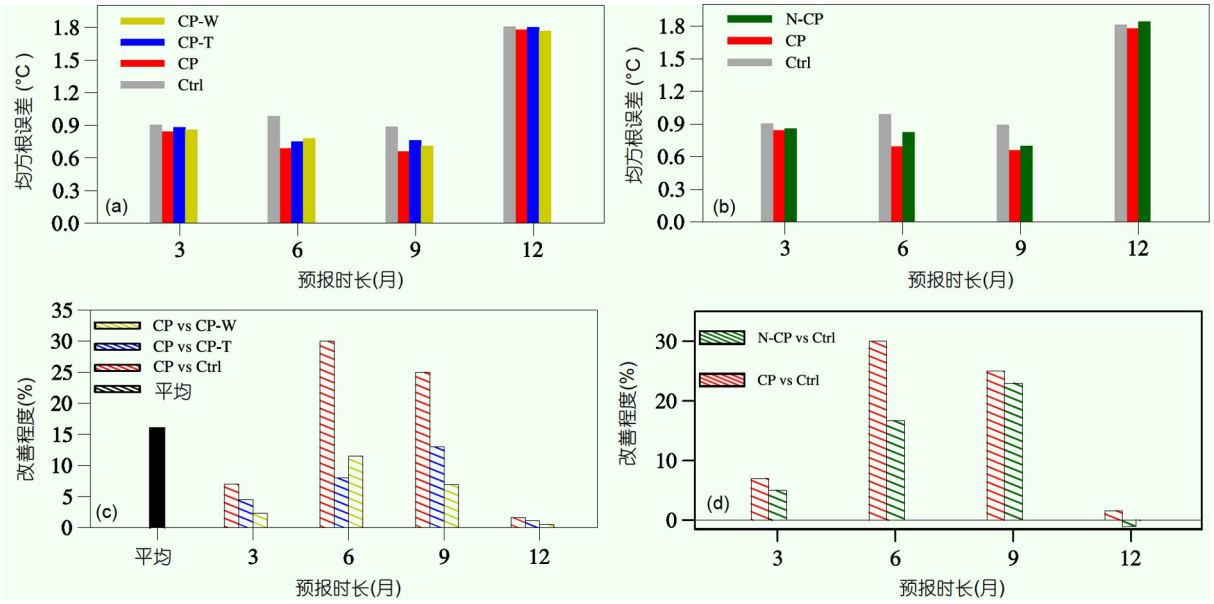

图 3　对ENSO成熟位相Niño3.4 SSTA的预报

(a) 控制预报以及CP、CP-T和CP-W集合平均预报的均方根误差; (b) 控制预报以及CP、N-CP集合平均预报的均方根误差; (c) 不同预报时长下CP-集合平均预报的均方根误差较控制预报(即“Ctrl”)的平均减小程度，及其较控制预报、CP-T和-W集合平均预报误差在不同超前预报时长下的减小程度. (d) CP、N-CP集合平均较控制预报的减小程度

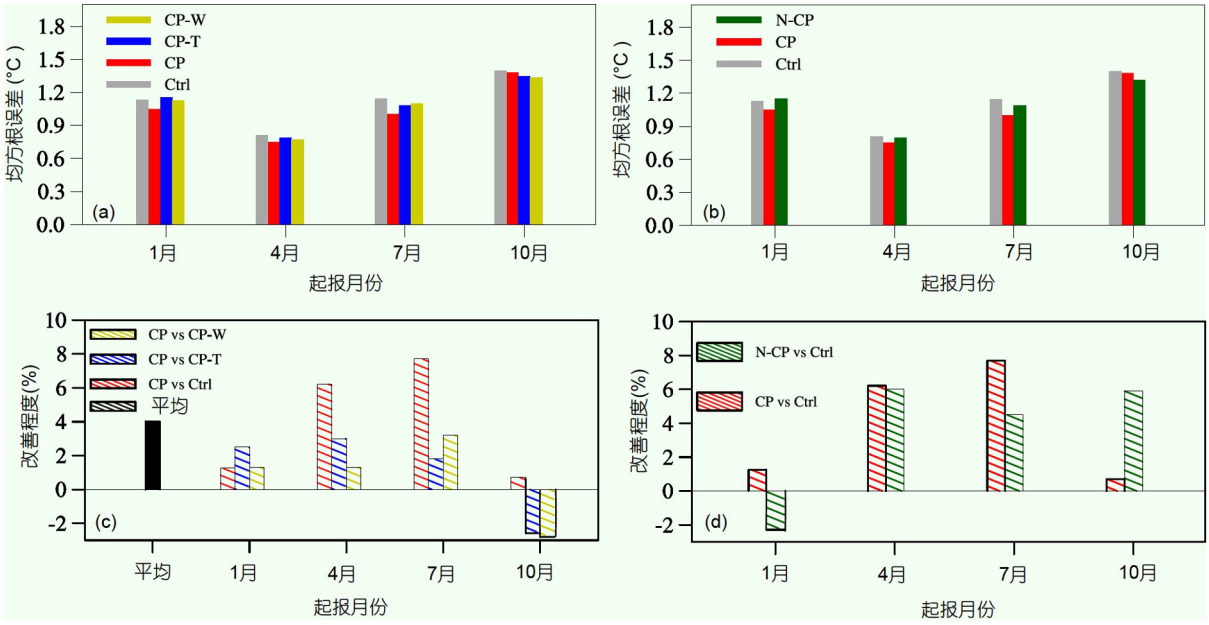

图 4　1982~2015期间Niño3.4 SSTA的预报

同图3, 但此处针对从不同季节开始, 预报时长为1年的预报

1996)，该噪音误差会被迅速放大，从而导致大的预报不确定性(Xue等，1994；Chen等，1995；Mu等，2007a，2007b)．然而，从上述结果可知，即使春夏季海气耦合强度最弱，耦合模式不易捕捉到该季节的弱耦合信号，但CP-集合平均预报在该季节起报时，获得了较控制预报、CP-T和-W集合平均预报显著高的预报技巧，从而

说明CP较CP-T和-W更恰当地描述了该季节弱海气耦合过程的不确定性.

3.3.2　距平相关系数

上节从Niño3.4 SSTA预报误差的角度衡量ENSO的预报技巧, 即主要关注ENSO 事件强度的预报不确定性. 本节将考察集合平均预报关于ENSO事件空间变率的预报技巧, 并采用距平相关系数(ACC)度量预报和观测的相似性.

图5给出了1982~2015年间所有El Niño和La Niña事件成熟位相SSTA空间变率预报的ACC的统计平均, 图6则提供了各类扰动集合平均预报与控制预报, 以及CP-集合平均与CP-T和-W集合平均预报关于成熟位相SSTA相关系数的差异. 结果表明, 无论是控制预报还是集合平均预报, 其相关系数均在热带中东太平洋区域最大, 但随着预报时长的增加, 相关系数逐渐降低(图5). 尽管这样, CP、CP-T和-W集合预报在超前预报时长为12月时, 在热带中东太平洋仍有较大区域的相关系数超过0.6, 而控制预报在超前12月预报时, 相关系数预报技巧几乎为零; 也就是说, 上述各类扰动的集合预报对ENSO事件成熟位相SSTA空间变率的预报, 较控制预报具有更高的预报技巧. 特别地, 从图6可以看出, CP-集合预报在赤道东南太平洋和热带西太平洋, 尤其当预报时长为12月时, 几乎在整个热带太平洋区域都维持着比控制预报更高的预报技巧, 而且较CP-T和-W集合预报也具有更高的相关系数(图6).

综上所述, 考虑初始海气耦合不确定性影响的CP-集合预报较未考虑初始耦合不确定性影响的CP-T和-W预报更有利于延长ENSO事件成熟位相SSTA空间变率的预报时效. 但需要说明的是, 图5表明CP-集合预报在超前12月对ENSO成熟位相SSTA预报时, 在热带中东太平洋具有超过0.6的距平相关系数, 该结果表明CP-集合预报在超前12月时捕捉到了热带中东太平洋SSTA的信号, 统计上对ENSO事件成熟位相SSTA具有较高的距平相关系数预报技巧, 但图2关于Niño3.4 SSTA的预报表明, CP-集合预报在超前9个月时可以捕捉到主要的El Niño和La Niña事件, 而在超前12月预报时, 虽然CP-集合预报捕捉到了大多数El Niño事件(见图2), 但它几乎没有预报出La Niña事件. 因此, 图5呈现的超前12个月对ENSO事件成熟位相SSTA预报的高距平相关系数, 主要体现在对El Niño的成功预报, 即是说, 综合预报误差和相关系数预报技巧的结果, 基于CESM模式的CP-集合预报对El Niño成熟位相SSTA具有更高预报技巧, 有效预报技巧可达12个月以上, 而对La Niña成熟位相SSTA的预报技巧为9个月.

3.4　初始扰动的耦合性质在提高ENSO集合预报技巧中的作用

CPs的海温和风场分量是在考虑它们耦合作用的情形下产生的, 彼此之间是动力协调的(如图1所示), 但如果将CP-T和-W简单组合同时扰动控制预报初始海温和风场, 那么该组合扰动虽然同时考虑了海温和风场初始不确定性, 但它们彼此之间动力作用并不协调(为方便, 记该类扰动为N-CP; 如图1所示). 如果将N-CP应用于ENSO集合预报, 将会对预报技巧产生何种影响呢? 该问题的回答将有助于揭示不同圈层初始扰动动力耦合在提高ENSO集合预报技巧中的作用.

我们采用N-CP作为集合预报初始扰动, 仍然对1982年1月~2015年12月期间的SSTA, 从每年的1、4、7、10月开始预报 1 年. 对每次预报, 与CP-集合预报类似, 我们产生5个N-CPs, 并以正负扰动对的形式叠加在控制预报的初始分析场产生10次扰动预报, 将该10次扰动预报与控制预报一起作为集合成员, 考察N-CP集合预报的技巧, 并与CP-集合预报比较, 揭示集合预报考虑初始耦合不确定性影响对提高ENSO集合预报技巧的作用.

图3给出了对ENSO成熟位相Niño3.4 SSTA的预报时, 控制预报、CP、N-CP集合平均预报的均方根误差, 以及CP、N-CP集合平均较控制预报预报误差的减小程度. 结果表明, 虽然N-CP集合平均与CP-集合平均类似, 在超前6个月和9个月时对控制预报的预报技巧的改善程度最大, 但CP-集合平均更大程度地提高了控制预报技巧, 尤其在超前6个月预报时, CP-集合平均较N-CP集合平均对控制预报的改善程度超过大约13.3%. 也就是说, 从春、夏季开始, 尤其从春季开始预报ENSO成熟位相Niño3.4 SSTA时, CP-集合平均较N-CP集合平均对控制预报技巧的改善具有更加明显的优势, 而从不同季节开始针对1982~2015期间每月SSTA预报一年时长时, 尽管CP-集合平均预报较N-CP集合平均预报对控制预报的改善程度没有预报成熟位

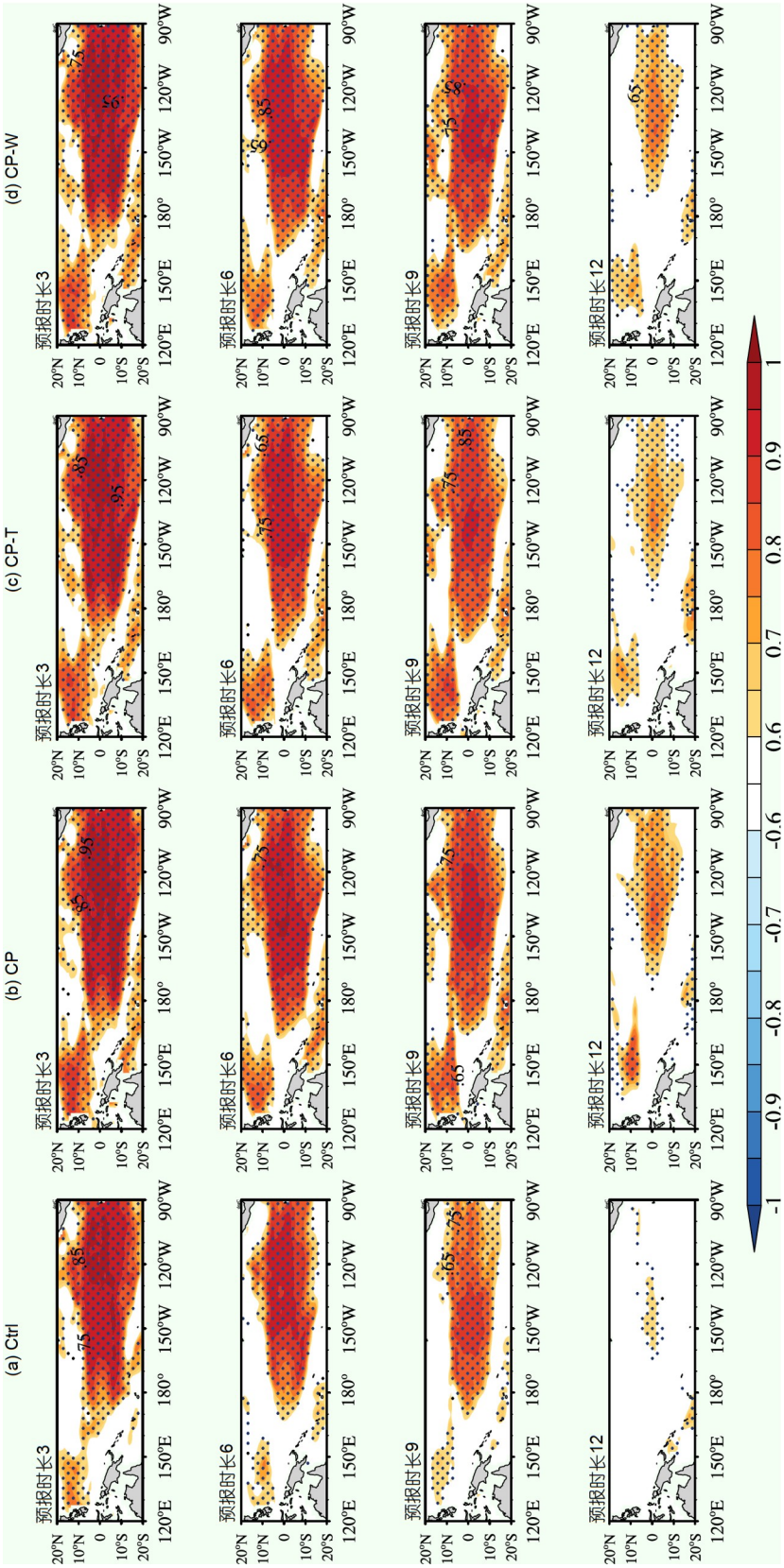

图 5 不同超前预报时长下, 对1982~2015年间El Niño和La Niña事件成熟位相SSTA空间变率预报的距平相关系数

(a) 控制预报; (b) CP-集合平均预报; (c) CP-T集合平均预报; (d) CP-W集合平均预报. 打点区域均已通过99%显著性检验

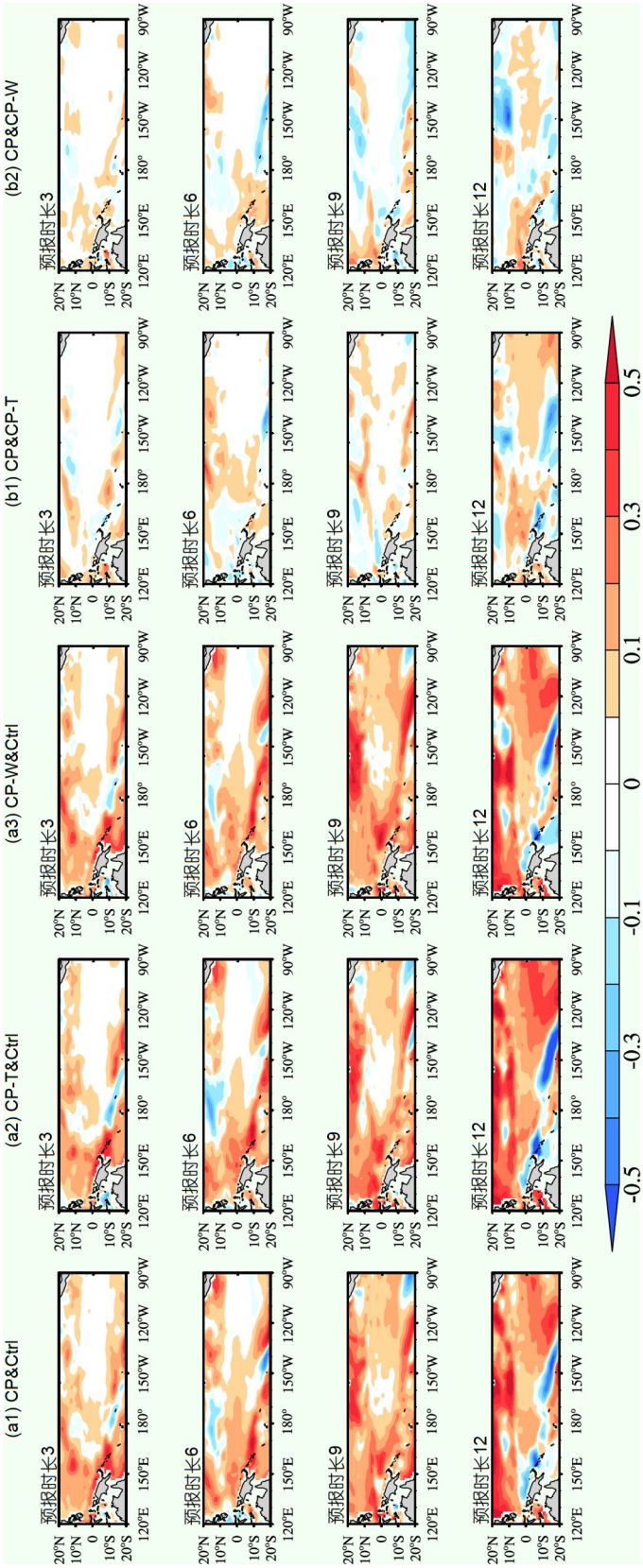

图 6　预报ENSO成熟位相SSTA的空间相关系数的差

(a1)–(a3)分别为CP、CP-T和-W集合平均预报与控制预报; (b1)和(b2)为CP-集合平均预报与CP-T和-W集合平均预报

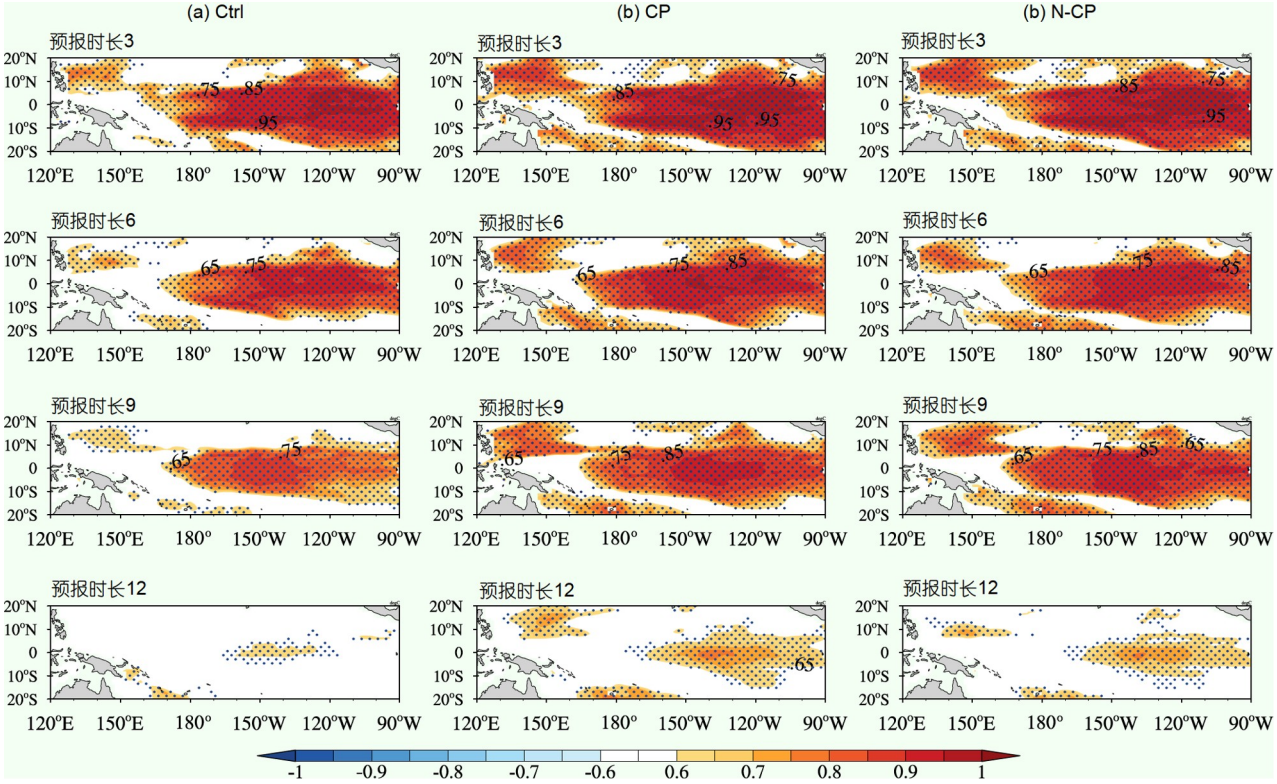

图 7　不同超前预报时长下, 对1982~2015年期间ENSO成熟位相SSTA空间变率预报的距平相关系数

(a) 控制预报; (b) CP-集合平均预报; (c) N-CP集合平均预报. 打点区域均已通过99%显著性检验

相Niño3.4 SSTA时更加显著, 但也常常更优(如图4所示).

对于ENSO事件成熟位相SSTA空间变率的预报, 我们发现无论是CP还是N-CP集合平均预报, 几乎在所有预报时长下均较控制预报在热带太平洋具有更高的相关系数预报技巧, 而当比较CP-和N-CP集合预报时, 发现CP-集合平均的预报技巧更高, 尤其在超前更长时间预报赤道两侧区域SSTA时体现得更为明显(见图7和8).

综上, 无论是Niño3.4 SSTA时间序列, 还是ENSO成熟位相SSTA空间变率的预报, CP-集合平均都较N-CP集合平均具有更高的预报技巧, 尤其从春夏季开始的预报, CP较控制预报和N-CP的优势更加明显. 因此, 考虑海-气动力协调相互作用的CP初始扰动, 能够促进集合平均预报延长ENSO的预报时效; 即使在春夏季海气耦合强度最弱的情形下, CP也能够捕捉到该弱耦合信号, 从而有效减少初始噪音造成的预报误差, 有效提高ENSO的预报技巧.

3.5　CP-集合预报的可靠性

Buizza等(2005)指出, 一个可靠的集合预报系统, 其集合离散度和集合平均预报均方根误差应近似相等. 事实上, 它们的比值越接近于1, 对应的集合预报系统提供的预报不确定性的估计越可靠. 图9给出了CP、CP-T和CP-W, 以及N-CP关于Niño3.4指数集合预报的RMSE和集合离散度(SPREAD)的比值(即 RMSE/SPREAD, 记为"可靠性指数"(RI))随预报时长的演变. 由图9可以看出, 尽管CP-集合预报的RI未能近似等于1, 但它几乎在所有预报时长下, 都较CP-T、CP-W和N-CP更靠近1. 因此, CP-集合预报较CP-T、CP-W和N-CP更可靠, 它提供的集合离散度更好地表征了热带太平洋Niño3.4区海温异常集合平均预报的预报误差. 图10给出了CP、CP-T和CP-W, 以及N-CP集合预报的RI在热带太平洋的空间分布. 由图可知, 各类扰动的集合预报在热带中东太平洋区域赤道以北大部分地区呈现的RI近似为1, 但在热带东南太平洋的RI则远超1, 近似等于2, 即使这样, CP集合预报的RI仍然较CP-T、

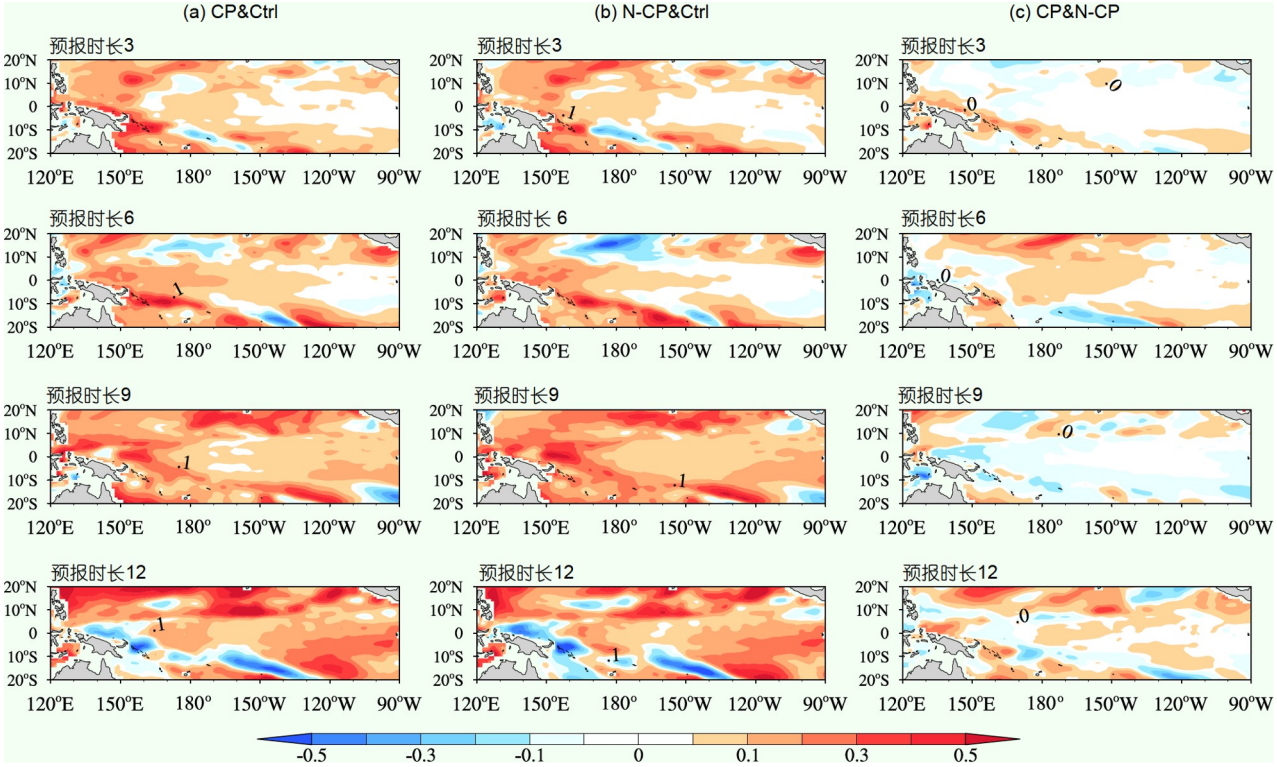

图 8　**关于ENSO成熟位相SSTA的空间距平相关系数的差**

(a) CP和N-CP集合平均预报与控制预报; (b) CP-集合平均预报与N-CP集合平均预报

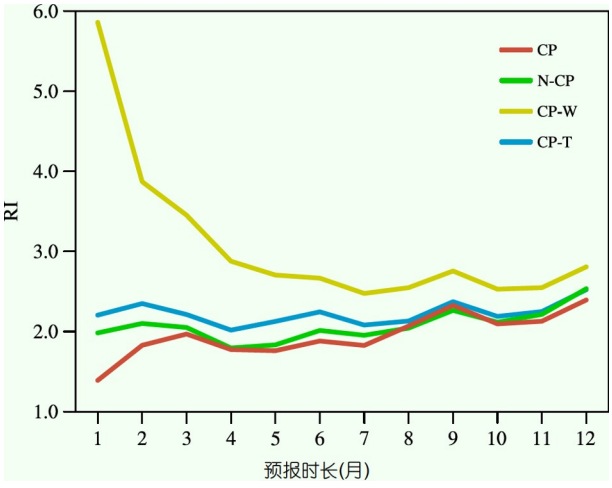

图 9　**CP、CP-T、CP-W和N-CP集合预报的可靠性指数的时间变率**

CP-W和N-CP更接近1. 所以, RI的空间分布也表明了CP-集合预报较CP-T、CP-W和N-CP能够更好地刻画热带中东太平洋SSTA预报的不确定性, 尤其较准确地反映了热带中东太平洋赤赤道以北区域SSTA的预报不确定性. 因此, CP-集合预报较CP-T、CP-W和N-CP具有更高的可靠性, 提供了更可靠的预报不确定性估计. Yang等(2012)表明, 当前关于气候变率的集合预报常常出现集合成员“过度自信”的现象, 即导致集合离散度显著小于集合平均预报误差(亦见Yang等, 2016和Liu等, 2019). 而上述结果表明, 由C-CNOP产生的耦合初始扰动增加了ENSO集合预报的集合离散度, 与集合平均预报误差差别更小, 从而提供了ENSO集合预报更可靠的集合成员. 所以, C-CNOP是一个能够产生耦合初始扰动, 减弱耦合系统集合预报“过度自信”现象的新方法, 而对上述研究, 我们期望未来在C-CNOP中包含更多相关变率不确定性相互作用的信息, 使ENSO集合预报的RI更加趋近1, 进一步提高ENSO集合预报的可靠性.

4　总结和讨论

传统的集合预报初始扰动方法未能很好考虑地球系统不同圈层相互作用的不确定性, 限制了耦合模式

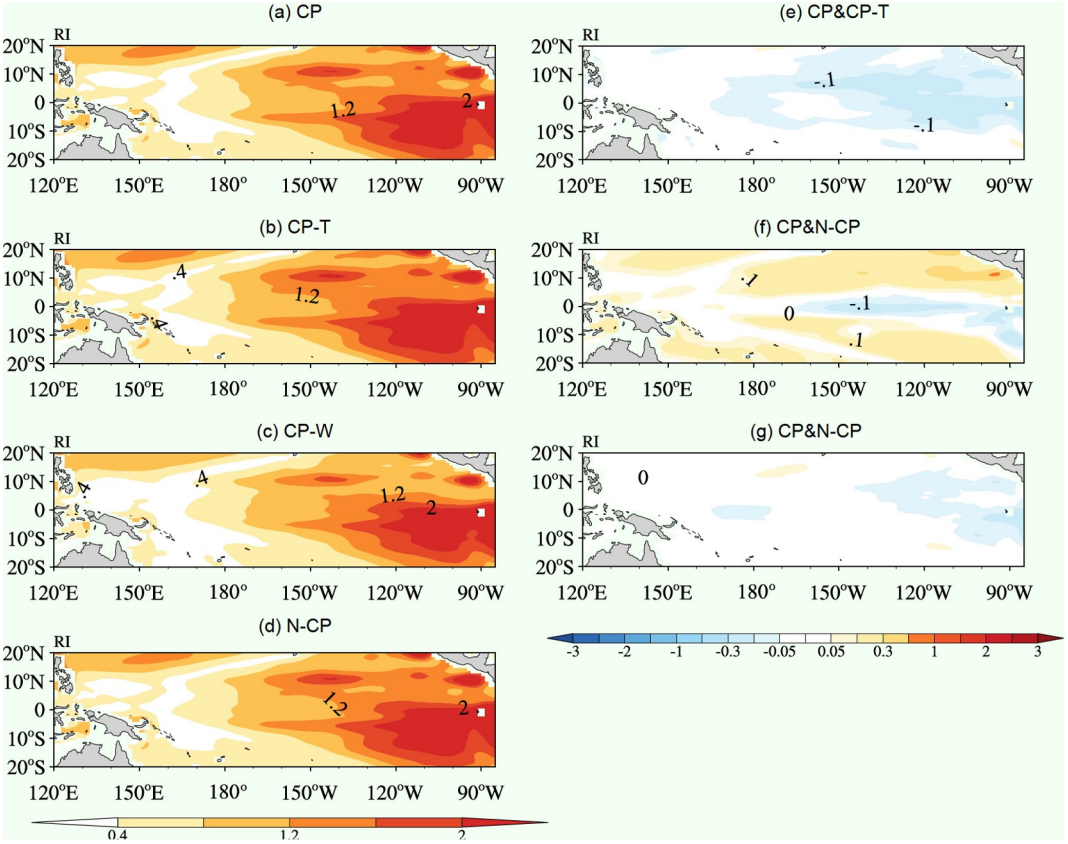

图 10　集合预报的可靠性指数的空间分布, 以及CP与集合预报可靠性指数的差

(a)~(d) CP、CP-T、CP-W和N-CP集合预报的可靠性指数的空间分布; (e)~(g) CP可靠性指数分别与CP-T, CP-W和N-CP的可靠性指数的差

集合预报水平的进一步提高. 该研究直接采用耦合模式输出资料的时间序列, 利用定常外强迫微分方程动力学解的性质, 提出了C-CNOP方法. C-CNOP考虑了地球系统不同圈层耦合的初始不确定性, 代表了预报时间段的非线性耦合快速增长初始扰动.

将C-CNOP方法应用于产生地球系统模式CESM集合预报的初始扰动, 对1982~2015年的海气耦合ENSO事件开展了集合预报试验, 从Niño3.4 SSTA时间变率和ENSO成熟位相SSTA空间变率两方面揭示了考虑初始耦合不确定性的C-CNOP在提高ENSO预报水平中的重要作用. 特别地, 由C-CNOP产生的集合预报耦合初始扰动成员CPs, 助力ENSO集合平均预报的预报误差显著低于控制预报, 尤其在春、夏季开始对ENSO成熟位相SSTA的预报, 预报误差减小甚至可达30%; 通过与分别扰动海洋温度(CP-T)和大气风场(CP-W)的集合预报相比, CP-集合预报对ENSO成熟位相SSTA的预报也具有更小的集合平均预报误差, 而且预报误差的最大减小程度同样发生在春、夏季开始的预报. 事实上, 热带太平洋在春季和夏初具有最弱的海气耦合强度, 从而使得耦合模式初始化更难刻画该季节的海气相互作用信息, 更容易产生大气和海洋噪音, 而该噪音误差由于该季节最强的海气耦合不稳定性更容易被迅速放大, 从而产生大的预报不确定性. 而CPs集合初始扰动较仅考虑初始海温扰动的CP-T和风场扰动的CP-W更好地描述了该季节弱海气耦合过程不确定性, 进而抑制了该季节误差的快速增长, 使CP-集合平均预报较CP-T和-W获得了更高的预报技巧. 对ENSO成熟位相SSTA空间变率的集合预报也表明, 考虑初始耦合不确定性影响的CP-集合预报较未考虑初始耦合不确定性影响的CP-T和-W预报更有利于延长ENSO事件成熟位相SSTA空间变率的预报时效. 因此, 无论从Niño3.4 SSTA预报误差的角度, 还是从ENSO成熟位相SSTA空间变率距平相关系数的角度, 均揭示了CP-集合平均预报的预报技巧显著高于控制预报、

CP-T和-W集合平均预报. 所以, 在ENSO预报中, 考虑初始海气耦合不确定性的影响对提高ENSO预报水平, 尤其对提高从春夏季开始的预报水平具有重要作用.

该研究也将CP-T和-W进行简单组合(记为N-CP), 组成了动力并不协调的海温和风场联合扰动模态. 用该联合模态同时扰动海温和风场开展了ENSO集合预报试验, 并与CP-集合预报进行了比较. 结果表明, CP较N-CP集合平均预报对控制预报的改善更加明显, 尤其体现在从春、夏季开始的预报; 当考察ENSO成熟位相SSTA空间变率集合预报的距平相关系数时, 发现CP-集合平均较N-CP集合平均预报具有更高的距平相关系数, 这种优势尤其体现在赤道两侧区域SSTA的超前更长时间的预报中. 因此, 恰当考虑初始海-气不确定性动力协调相互作用的CPs, 能够有效延长ENSO的预报时效, 尤其能够有效捕捉春、夏季的弱海气耦合信号, 从而减少该季节初始噪音任意放大引起的预报误差的影响.

该研究对CP-集合预报提供的不确定性估计进行了可靠性评估. 结果表明, 无论从时间变率还是空间变率, CP-集合预报都较CP-T、CP-W和N-CP能够更好地刻画集合平均预报误差和集合离散度之间的一致性关系, 尤其在热带中东太平洋赤道以北区域, CP-集合预报呈现了更强的可靠性. 因此, 对ENSO预测, 更恰当考虑初始海气耦合不确定性的CP-集合预报, 较CP-T、CP-W和N-CP能够更可靠地估计集合平均预报的不确定性. 所以, C-CNOP提供了一个有利于克服气候系统集合预报“过度自信”现象的初始扰动新方法.

综上, 由C-CNOP产生的耦合快速增长初始扰动CPs, 更好地刻画了初始海洋和大气不确定性的动力协调相互作用对ENSO集合预报的影响, 使得ENSO获得了更高的集合平均预报水平, 特别是从春、夏季开始的具有更高预报技巧的ENSO预报, 更加彰显了C-CNOP捕捉初始海气耦合不确定信息的巨大潜力. 但这里需要指出的是, 上述结论主要针对集合平均预报结果, 即主要关注了C-CNOP方法在提高集合预报确定性预报技巧中的重要作用. 然而, 上述C-CNOP对确定性预报技巧的显著提高鼓舞我们进一步采用更多的ENSO事件或更长的时间序列, 考察C-CNOP对促进集合预报概率预报技巧的作用. 另外, 考虑到C-CNOP是一个新提出的集合预报扰动方法, 为了快速证明C-CNOP动力学的合理性, 同时也为了节省集合预报计算量, 我们初步尝试了较少的扰动样本进行集合预报试验, 即使这样, C-CNOP较单纯的大气或海洋扰动, 或者由它们组合的初始海气联合扰动, 也具有更高的集合预报技巧. 那么, 究竟应该采用多少样本数才能使得耦合模式的C-CNOP集合预报达到最高水平, 在此情形下, 是否C-CNOP较其他扰动方式在提高集合预报水平中具有更加明显的优势, 集合平均预报的均方根误差和离散度的一致性关系是否变得更为可靠? 等等这些问题, 需要未来进一步深入研究. 另外, 如何将C-CNOP方法与未能恰当考虑不同圈层耦合初始不确定性的SVs和BVs进行合理比较, 也是未来需要考虑的问题. 总之, 我们希望在继续深入研究的基础上, 将C-CNOP发展成为一个具有深厚理论基础且能获得更高预报技巧的耦合模式集合预报新方法.

参考文献

Baehr J, Piontek R. 2014. Ensemble initialization of the oceanic component of a coupled model through bred vectors at seasonal-to-interannual timescales. Geosci Model Dev, 7: 453–461

Buizza R, Palmer T N. 1995. The singular-vector structure of the atmospheric global circulation. J Atmos Sci, 52: 1434–1456

Buizza R, Houtekamer P L, Pellerin G, Toth Z, Zhu Y, Wei M. 2005. A comparison of the ECMWF, MSC, and NCEP global ensemble prediction systems. Mon Weather Rev, 133: 1076–1097

Chen D, Zebiak S E, Busalacchi A J, Cane M A. 1995. An improved procedure for EI Niño forecasting: Implications for predictability. Science, 269: 1699–1702

Craig A P, Vertenstein M, Jacob R. 2012. A new flexible coupler for earth system modeling developed for CCSM4 and CESM1. Int J High Perform Comput Appl, 26: 31–42

Du H, Doblas-Reyes F J, García-Serrano J, Guemas V, Soufflet Y, Wouters B. 2012. Sensitivity of decadal predictions to the initial atmospheric and oceanic perturbations. Clim Dyn, 39: 2013–2023

Du J, Berner J, Buizza R, Charron M, Houtekamer P, Hou D, Jankov I, Mu M, Wang X G, Wei M Z, Yuan H L. 2018. Ensemble Methods for Meteorological Predictions. Handbook of Hydrometeorological Ensemble Forecasting. Spring. 1–52

Du J, Zhou B, Levit J. 2019. Measure of forecast challenge and predictability horizon diagram index for ensemble models. Weather Forecast, 34: 603–615

Duan W, Liu X, Zhu K, Mu M. 2009. Exploring the initial errors that cause a significant “spring predictability barrier” for El Niño events. J Geophys Res, 114: 2008JC004925

Duan W, Wei C. 2013. The 'spring predictability barrier' for ENSO predictions and its possible mechanism: Results from a fully coupled model. Intl J Clim, 33: 1280–1292

Duan W, Huo Z. 2016. An approach to generating mutually independent initial perturbations for ensemble forecasts: Orthogonal conditional nonlinear optimal perturbations. J Atmos Sci, 73: 997–1014

Duan W S, Mu M. 2018. Predictability of El Niño-Southern Oscillation Events. Oxford Research Encyclopedia of Climate Science

Duan W, Feng R, Yang C, Jiang L. 2022. A new approach to data assimilation for numerical weather forecasting and climate prediction. J Appl Anal Comput, 12: 1007–1021

Duan W, Yang L, Mu M, Wang B, Shen X, Meng Z, Ding R. 2023a. Recent advances in China on the predictability of weather and climate. Adv Atmos Sci, 40: 1521–1547

Duan W S, Yang L C, Xu Z Z, Chen J. 2023b. Conditional nonlinear optimal perturbation: Applications to ensemble forecasting of high-impact weather systems. In: Seon Ki Park, ed. Numerical Weather Prediction: East Asian Perspectives. Springer Atmos Sci, 17: 441–460

Hou M, Duan W, Zhi X. 2019. Season-dependent predictability barrier for two types of El Niño revealed by an approach to data analysis for predictability. Clim Dyn, 53: 5561–5581

Hunke E C, Lipscomb W H, Turner A K, Jeffery N, Elliott S. 2008. The Los Alamos sea ice model documentation and software users manual. Version 4.0. Los Alamos National Laboratory

Huo Z, Duan W. 2018. The application of the orthogonal conditional nonlinear optimal perturbations method to typhoon track ensemble forecasts. Sci China Earth Sci, 62: 376–388

Huo Z, Duan W, Zhou F. 2019. Ensemble forecasts of tropical cyclone track with orthogonal conditional nonlinear optimal perturbations. Adv Atmos Sci, 36: 231–247

Kleeman R, Tang Y, Moore A M. 2003. The calculation of climatically relevant singular vectors in the presence of weather noise as applied to the ENSO problem. J Atmos Sci, 60: 2856–2868

Lian T, Wang J, Chen D, Liu T, Wang D. 2023. A strong 2023/24 El Niño is staged by Tropical Pacific Ocean heat content buildup. Ocean-Land-Atmos Res, 2: 0011

Liu T, Tang Y, Yang D, Cheng Y, Song X, Hou Z, Shen Z, Gao Y, Wu Y, Li X, Zhang B. 2019. The relationship among probabilistic, deterministic and potential skills in predicting the ENSO for the past 161 years. Clim Dyn, 53: 6947–6960

Molteni F, Buizza R, Palmer T N, Petroliagis T. 1996. The ECMWF ensemble prediction system: Methodology and validation. Quart J R Meteoro Soc, 122: 73–119

Mu M, Duan W S, Wang B. 2003. Conditional nonlinear optimal perturbation and its applications. Nonlin Process Geophys, 10: 493–501

Mu M, Xu H, Duan W. 2007a. A kind of initial errors related to "spring predictability barrier" for El Niño events in Zebiak-Cane model. Geophys Res Lett, 34: 2006GL027412

Mu M, Duan W, Wang B. 2007b. Season-dependent dynamics of nonlinear optimal error growth and El Niño-Southern Oscillation predictability in a theoretical model. J Geophys Res, 112: 2005JD006981

Mureau R, Molteni F, Palmer T N. 1993. Ensemble prediction using dynamically conditioned perturbations. Quart J R Meteoro Soc, 119: 299–323

Neale R B, Richter J H, Conley A J, Park S, Lauritzen P H, Gettelman A,Williamson D L, Rasch P J,Vavrus S J,Taylor M A, Collins W D, Zhang M H, Lin S J. 2010. Description of the NCAR Community Atmosphere Model (CAM5. 0). Technical Report. Note NCAR/TN-486+ STR, 1: 1–12

Oleson K W, Lawrence D M, Bonan G B, Flanner M G, Kluzek E, Lawrence P J, Levis S, Swenson S C, Thornton P E, Dai A, Decker M, Dickinson R, Feddema J, Heald C L, Hoffman F, Lamarque J F, Mahowald N, Niu G Y, Qian T, Randerson J, Running S, Sakaguchi K, Slater A, Stöckli R, Wang A, Yang Z, Zeng X D, Zeng X B. 2010. Technical description of version 4.0 of the Community Land Model (CLM). Technical Report. National Center for Atmospheric Research

Smith R, Jones P, Briegleb B, Bryan F, Danabasoglu G, Dennis J, Dukowicz J, Eden C, Fox-Kemper B, Gent P, Hecht M, Jayne S, Jochum M, Large W, Lindsay K, Maltrud M, Norton N, Peacock S, Vertenstein M, Yeager S. 2010. The parallel ocean program (POP) reference manual ocean component of the community climate system model (CCSM) and community earth system model (CESM). LAUR-01853, 141: 1–140

Tang Y, Zhang R H, Liu T, Duan W, Yang D, Zheng F, Ren H, Lian T, Gao C, Chen D, Mu M. 2018. Progress in ENSO prediction and predictability study. Natl Sci Rev, 5: 826–839

Toth Z, Kalnay E. 1993. Ensemble forecasting at NMC: The generation of perturbations. Bull Amer Meteor Soc, 74: 2317–2330

Vannitsem S, Duan W. 2020. On the use of near-neutral Backward Lyapunov Vectors to get reliable ensemble forecasts in coupled ocean-atmosphere systems. Clim Dyn, 55: 1125–1139

Wang B, Fang Z. 1996. Chaotic oscillations of tropical climate: A dynamic system theory for ENSO. J Atmos Sci, 53: 2786–2802

Webster P J, Yang S. 1992. Monsoon and Enso: Selectively interactive systems. Quart J R Meteoro Soc, 118: 877–926

Webster P J. 1995. The annual cycle and the predictability of the tropical coupled ocean-atmosphere system. Meteorl Atmos Phys,

56: 33–55

Xie S P, Philander S G H. 1994. A coupled ocean-atmosphere model of relevance to the ITCZ in the eastern Pacific. Tellus A-Dynam Meteor Oceanogr, 46: 340–350

Xue Y, Cane M A, Zebiak S E, Blumenthal M B. 1994. On the prediction of ENSO: A study with a low-order Markov model. Tellus A-Dynam Meteor Oceanogr, 46: 512–528

Yan L, Yu Y, Wang B, Li L, Wang P. 2009. ENSO hindcast experiments using a coupled GCM. Atmos Ocean Sci Lett, 2: 7–13

Yang D, Tang Y, Zhang Y, Yang X. 2012. Information-based potential predictability of the Asian summer monsoon in a coupled model. J Geophys Res, 117: 2011JD016775

Yang D, Yang X, Xie Q, Zhang Y, Ren X, Tang Y. 2016. Probabilistic versus deterministic skill in predicting the western North Pacific-East Asian summer monsoon variability with multimodel ensembles. J Geophys Res-Atmos, 121: 1079–1103

Zhang H, Duan W, Zhang Y. 2023. Using the orthogonal conditional nonlinear optimal perturbations approach to address the uncertainties of tropical cyclone track forecasts generated by the WRF model. Weather Forecast, 38: 1907–1933

Zheng F, Zhu J. 2010. Coupled assimilation for an intermediated coupled ENSO prediction model. Ocean Dyn, 60: 1061–1073

(责任编委: 雷荔傈)